

ASR: Attention-alike Structural Re-parameterization

Shanshan Zhong^{1*}, Zhongzhan Huang^{1*}, Wushao Wen¹, Jinghui Qin^{2†}, Liang Lin¹

¹School of Computer Science and Engineering, Sun Yat-sen University

²School of Information Technology, Guangdong University of Technology

Abstract

The structural re-parameterization (SRP) technique is a novel deep learning technique that achieves interconversion between different network architectures through equivalent parameter transformations. This technique enables the mitigation of the extra costs for performance improvement during training, such as parameter size and inference time, through these transformations during inference, and therefore SRP has great potential for industrial and practical applications. The existing SRP methods have successfully considered many commonly used architectures, such as normalizations, pooling methods, and multi-branch convolution. However, the widely used attention modules which drastically slow inference speed cannot be directly implemented by SRP due to these modules usually act on the backbone network in a multiplicative manner and the modules' output is input-dependent during inference, which limits the application scenarios of SRP. In this paper, we conduct extensive experiments from a statistical perspective and discover an interesting phenomenon *Stripe Observation*, which reveals that channel attention values quickly approach some constant vectors during training. This observation inspires us to propose a simple-yet-effective attention-alike structural re-parameterization (ASR) that allows us to achieve SRP for a given network while enjoying the effectiveness of the attention mechanism. Extensive experiments conducted on several standard benchmarks demonstrate the effectiveness of ASR in generally improving the performance of existing backbone networks, attention modules, and SRP methods without any elaborated model crafting. We also analyze the limitations and provide experimental and theoretical evidence for the strong robustness of the proposed ASR.

1 Introduction

The structural re-parameterization (SRP) technique (Guo, Alvarze, and Salzmann 2020; Cao et al. 2020; Ding et al. 2021d; Hu et al. 2022; Wang, Dong, and Shan 2022) is an efficient neural network technology that decouples training and inference, greatly facilitating the deployment of Deep Neural Networks (DNNs) in practical applications and possessing excellent potential for industrial implementation. During the training phase, SRP increases the model's representation power for a given backbone network by adding

*These authors contributed equally.

†Corresponding author.

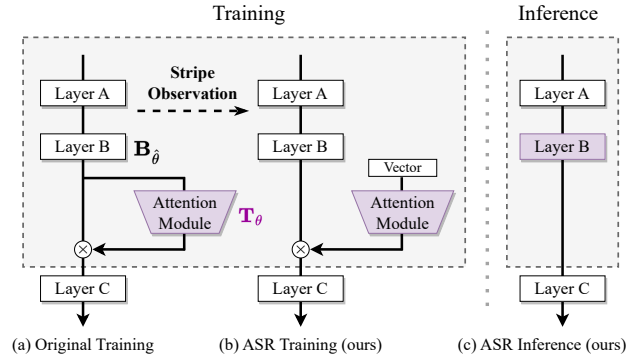


Figure 1: The sketch of ASR. Inspired by *Stripe Observation*, we utilize a learnable vector as input to the attention module for training. In Inference phase, the attention module can be merged into the parameters of the backbone.

multiple branches or specific layers with various neural network components to the backbone. During the inference phase, the added branches or layers can be merged into the parameters of the backbone network through some equivalent transformations, enabling performance improvement without any additional parameters or computational costs. Specifically, for an input x , a branch layer \mathbf{T}_θ with learnable parameters θ , and a layer on the backbone \mathbf{B}_β (usually a convolutional filter with a sufficiently large kernel size (Ding et al. 2021c)), if there are transformations h and g such that

$$\underbrace{h[\mathbf{T}_\theta, \mathbf{B}_\beta]}_{\text{Training}}(x) = \underbrace{\mathbf{B}_{g[\hat{\theta}, \theta]}}_{\text{Inference}}(x), \quad (1)$$

this situation can be decoupled in training and inference processing using SRP. For example, during training, $\mathbf{Conv}_\theta(x) + \mathbf{Conv}_\beta(x)$ can be equivalently transformed into $\mathbf{Conv}_{\theta+\hat{\theta}}(x)$ during inference, enabling the model performance of two convolutional filters to be achieved with only one convolutional filter. Another example about batch normalization (BN) is $\mathbf{BN}_\theta(\mathbf{Conv}_\beta(x))$ can be equivalently transformed into $\mathbf{Conv}_{\hat{\theta}, a, b}(x)$ during inference, where a and b are constants related to θ . Based on the idea of Eq.(1), although previous SRP methods have successfully integrated various neural network components, including normalization methods, multi-branch convolution, global pooling, etc., existing methods are currently unable

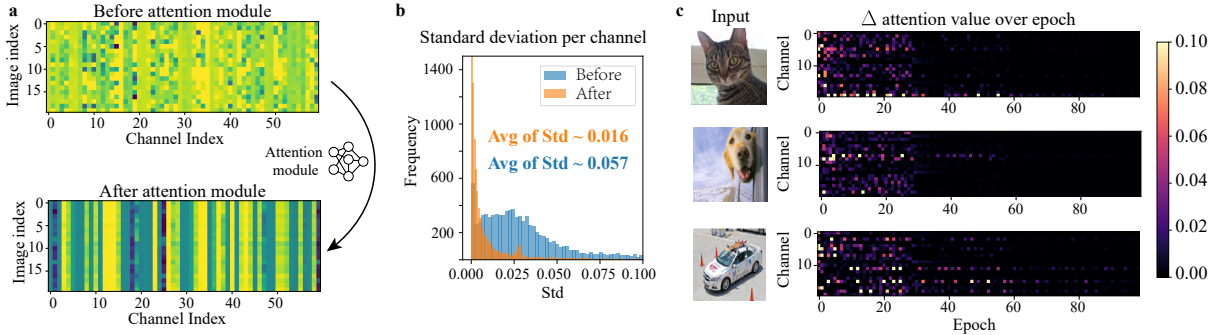


Figure 2: The visualization of the *Stripe Observation* (see appendix for more examples). **a**, after passing through the attention model, the attention values of different images tend to approach a certain value within the same channel, resulting in a “stripe structure”. **b**, the standard deviation of attention values for each channel is almost distributed around zero. **c**, the visualization of the first-order difference (absolute value) for attention value over epoch. Most of the values approach a constant rapidly.

to be applied to attention modules, which are widely used in deep learning applications. This is due to the fact that the attention module \mathbf{T}_θ , as illustrated in Fig.1 (a), acts on the backbone network in a multiplicative manner (usually is the element-wise multiplication \odot), and the module’s output is also input-dependent during inference. For these reasons, usually, for a given transformation g , we have

$$\mathbf{B}_{\hat{\theta}} \odot \mathbf{T}_\theta \neq \mathbf{B}_{g[\hat{\theta}, \theta]}. \quad (2)$$

Eq.(2) reveals that the attention module is not directly compatible with the existing SRP’s paradigm, which means that the widely used attention networks may limit the scenarios and scope of SRP. However, attention modules have an unignorable impact on inference. Despite their few parameters, attention modules can drastically slow inference speed due to complex computations. Table 1 shows there is a decrease in average frames per second (FPS) of more than 36% with attention use. Therefore, there is a question: **Can we incorporate the effectiveness of attention mechanisms into SRP in an indirect way?**

Model	CIFAR100		STL10	
	#param.	FPS	#param.	FPS
ResNet164	1.73M	1944	1.70M	255
+IE	1.74M	1505 (↓ 22.56%)	1.72M	170 (↓ 33.26%)
+SRM	1.76M	1387 (↓ 28.64%)	1.74M	162 (↓ 36.40%)
+CBAM	1.93M	793 (↓ 59.21%)	1.90M	127 (↓ 50.23%)
+SE	1.93M	1469 (↓ 24.42%)	1.91M	173 (↓ 32.08%)
+DIA	1.95M	1092 (↓ 43.82%)	1.92M	211 (↓ 17.20%)
+SPA	3.86M	1080 (↓ 44.45%)	3.83M	180 (↓ 29.36%)

Table 1: The significant decrease in inference speed by using attention modules for the backbone network.

To answer this question, we first propose a counter-intuitive phenomenon that occurs in different datasets, network structures, and channel attention modules, that is

(Stripe Observation) As shown in Fig.2, the attention value $\mathbf{v}_i \in \mathbb{R}^c$ obtained by i -th channel attention module will rapidly approach to a value $\bar{\mathbf{v}}_i \in \mathbb{R}^c$, which $\bar{\mathbf{v}}_i$ may follow a distribution with mean vector μ_i and covariance matrix $\text{diag}(\sigma_{i1}^2, \dots, \sigma_{ic}^2)$, σ_{ij} , $j = 1, 2, \dots, c$ closes to 0.

Empirically, as shown in Fig.2, we visualize the attention values of the well-known attention module SE (Hu, Shen, and Sun 2018) on the ResNet50 (He et al. 2016) architecture trained on the ImageNet (Russakovsky et al. 2015) dataset to observe the so-called *Stripe Observation*. For Fig.2 **a**, we randomly select 20 images from the ImageNet dataset as inputs to the model and visualize the values of feature maps before and after passing through the attention module. Here, we only show 60 channels randomly selected from all channels. We find that the values of the input feature maps of the attention module varied greatly among different channels and images, while the output values of different images generated from the attention module tended to approach a certain value within the same channel, resulting in a “stripe structure”. Therefore, we call this phenomenon *Stripe Observation*. Further, we can quantify this observation from a statistical perspective. Specifically, we visualize the standard deviation of values for each channel of the feature map before and after passing through the attention modules, as shown in Fig.2 **b**. We observe that the standard deviation of values for each channel is almost distributed around zero after passing through the attention module, regardless of the images, indicating that the attention values at any module do indeed approach a corresponding constant vector. Let \mathbf{v}_i^t be the attention value obtained by the i -th module during the t -th epoch, We can further explore the process of forming these constant vectors. Fig.2 **c** visualizes the first-order difference (absolute value) of three input images over epoch for randomly selected 20 channels, i.e., $\Delta_i = \text{abs}[\mathbf{v}_i^{t+1} - \mathbf{v}_i^t]$. Typically, a commonly used schedule learning rate is applied for training ResNet50 on the ImageNet dataset, where the learning rate is reduced by 90% every 30 epochs. As shown in Fig.2 **c**, most of the values almost converge at the first learning rate decay (30 epochs), i.e., the first-order difference is zero (black color). More empirical visualizations about *Stripe Observation* can be found in the appendix.

Inspired by the *Stripe Observation* that the channel attention values of different inputs in a dataset tend to approach a constant vector, we propose an Attention-like Structural Re-parameterization (ASR) as shown in Fig.1 (b), where we directly consider a learnable vector as the input to the atten-

tion modules. This makes the attention modules relatively independent of the model input so that the ‘‘attention values’’ become a constant vector after training. Therefore, the dilemma mentioned in Eq.(2) is solved, and we can achieve the SRP, like Fig.1 (c), of a given model while enjoying the effectiveness of the attention mechanism. The details of ASR can be found in Section 3. We also demonstrate the effectiveness of ASR and its compatibility with existing neural network training methods using multiple benchmarks in Section 4. Furthermore, we provide the empirical and theoretical evidence for the strong robustness of ASR in Section 6. We summarize the contributions as follows:

- We revisit the channel attention mechanism from a statistical perspective. With comprehensive experiments, we find the *Stripe Observation*, which reveals that the attention value approach constant vectors during training.
- We coin a novel structural re-parameterization method ASR, tailored for *Stripe Observation*, which can leverage various attention modules to improve the model performance without extra parameters and inference time.
- We provide experimental and theoretical evidence for the proposed ASR’s compatibility, effectiveness, and robustness. Besides, we also point out the limitations of ASR.

2 Related works

Attention mechanism. It selectively focuses on the most informative components of a network via self-information processing and has gained a promising performance on vision tasks (Liang et al. 2020). For example, SENet (Hu, Shen, and Sun 2018) proposes the channel attention mechanism, which adjusts the feature map with channel view, and CBAM (Woo et al. 2018) considers both channel and spatial attention for adaptive feature refinement. Recently, more works (Fu et al. 2019; Hou, Zhou, and Feng 2021; Zhu et al. 2019; Gao et al. 2019; Cao et al. 2019; Zhang et al. 2020; Qin et al. 2021) are proposed to optimize spatial attention and channel attention. Most of the above works regard the attention mechanism as an additional module of the backbone network, and with the development of the transformer (Vaswani et al. 2017), a large number of works (Yu et al. 2022; Dosovitskiy et al. 2020; Touvron et al. 2022) regard the attention as a part of the backbone network.

Structural re-parameterization. It enables different architectures to be mutually converted through the equivalent transformation of parameters (Hu et al. 2022). For instance, a branch of 1×1 convolution and a branch of 3×3 convolution can be transferred into a single branch of 3×3 convolution (Ding et al. 2021d). In the training phase, multi-branch (Ding et al. 2021c,d) and multi-layer (Guo, Alvarze, and Salzmann 2020; Cao et al. 2020) topologies are designed to replace the vanilla layers for augmenting models. Afterward, during inference, the training-time complex models are transferred to simple ones for faster inference. Cao et al (Cao et al. 2020) have discussed how to merge a depthwise separable convolution kernel during training. Thanks to the efficiency of structural re-parameterization, it has gained great importance and has been utilized in various tasks (Huang et al. 2022; Luo, Si, and Deng 2022; Zhou

et al. 2022; Zhang et al. 2022) such as compact model design (Dosovitskiy et al. 2020), architecture search (Chen et al. 2019; Zhang et al. 2021), pruning (Ding et al. 2021a), image recognition (Ding et al. 2021b), and super-resolution (Wang, Dong, and Shan 2022; Gao et al. 2023).

3 Proposed method

Our attention-alike structural re-parameterization (ASR) is a simple-yet-effective method without introducing any additional computational cost and parameters in inference, which can share the effectiveness of any channel attention module by considering a learnable vector as input for the attention module. Fig. 1 depicts the sketch of ASR. In the following subsections, we first introduce the preliminary channel attention modules in Section 3. We then detail discuss the training and inference phase of ASR in Section 3.

Preliminary: channel attention in vision

Given a single input $\mathbf{x} \in \mathbb{R}^{C\times H\times W}$ of channel attention modules (see Fig.1), we usually obtain the corresponding global information $\mathbf{u} \in \mathbb{R}^{C\times 1\times 1}$ through global average pooling (GAP) following (Hu, Shen, and Sun 2018; Huang et al. 2020; Zhong, Wen, and Qin 2022), where the c -th element of \mathbf{u} is calculated as follows:

$$\mathbf{u}_c = \text{GAP}(\mathbf{x}_c) = \frac{1}{H \times W} \sum_{i=1}^H \sum_{j=1}^W \mathbf{x}_{c,i,j}. \quad (3)$$

Then, the attention value $\mathbf{v} \in \mathbb{R}^{C\times 1\times 1}$ is calculated and leveraged to adjust the input \mathbf{x} using Eq.(4).

$$\mathbf{x}' = \mathbf{x} \odot \mathbf{v}, \text{ where } \mathbf{v} = \mathbf{T}_\theta(\mathbf{u}) = \sigma(\mathcal{F}_\theta(\mathbf{u})), \quad (4)$$

where \odot denotes channel-wise multiplication, \mathcal{F}_θ is the neural network part of attention modules with learnable parameters θ , and $\sigma(\cdot)$ is activation function.

Attention-alike structural re-parameterization

Training phase. Based on *Stripe Observation*, we can directly consider a learnable vector $\psi \in \mathbb{R}^{C\times 1\times 1}$ as the input of \mathcal{F}_θ . Without GAP, we measure the output of attention modules by $\mathbf{v}_{\psi,\theta} = \sigma(\mathcal{F}_\theta(\psi)) \in \mathbb{R}^{C\times 1\times 1}$. Then during the training phase, ψ will be simultaneously updated with other learnable parameters.

Inference phase. After training, according to the paradigm of SRP, we consider equivalently merging the attention module into the backbone, as shown in Fig.1 (c). Since the ‘‘attention value’’ $\mathbf{v}_{\psi,\theta}$ is a constant vector, for the various common-used modules \mathbf{B}_θ in backbone, we can seamlessly find the corresponding transformation \mathcal{g} such that

$$\mathbf{B}_\theta \odot \mathbf{v}_{\psi,\theta} = \mathbf{B}_{g[\hat{\theta},\psi,\theta]}, \quad (5)$$

for example, for input \mathbf{x} , if \mathbf{B}_θ is a convolutional layer \mathcal{C} with kernels \mathbf{K} and bias \mathbf{b} , then Eq.(5) can be rewritten as

$$\begin{aligned} \mathcal{C}(\mathbf{x}; \mathbf{K}, \mathbf{b}) \odot \mathbf{v}_{\psi,\theta} &= \mathbf{x} * \mathbf{K} \odot \mathbf{v}_{\psi,\theta} + \mathbf{b} \odot \mathbf{v}_{\psi,\theta} \\ &= \mathcal{C}(\mathbf{x}; \mathbf{K} \odot \mathbf{v}_{\psi,\theta}, \mathbf{b} \odot \mathbf{v}_{\psi,\theta}), \end{aligned} \quad (6)$$

where $*$ denote convolution and $\mathbf{K} \odot \mathbf{v}_{\psi,\theta}$ means that the product of i -th elements of $\mathbf{v}_{\psi,\theta}$ and i -th kernel of \mathbf{K} .

Since the existing SRP methods mainly merge various neural network layers into a convolutional layer, from Eq.(6), ASR is compatible with most of these SRP methods. Moreover, since the channel attention module is generally placed after the normalization layer, we can also take batch normalization **BN** as an example, i.e.,

$$\begin{aligned} \mathbf{BN}(\mathbf{x}; \gamma, \beta) \odot \mathbf{v}_{\psi, \theta} &= \frac{(\mathbf{x} - \mu) \odot \gamma \odot \mathbf{v}_{\psi, \theta}}{\sigma} + \beta \odot \mathbf{v}_{\psi, \theta} \\ &= \mathbf{BN}(\mathbf{x}; \gamma \odot \mathbf{v}_{\psi, \theta}, \beta \odot \mathbf{v}_{\psi, \theta}), \end{aligned} \quad (7)$$

where μ, σ, γ , and β are the accumulated mean, standard deviation, and learned scaling factor and bias of **BN**, respectively. See the appendix for more of the equivalent transformations for other $\mathbf{B}_{\hat{\theta}}$.

Model	#param.	Image size	Top-1
ResNet34	22M	224 ²	73.31
ResNet34+ASR (SE)	22M	224 ²	74.04 (↑ 0.73)
ResNet34+ASR (ECA)	22M	224 ²	73.88 (↑ 0.57)
ResNet34+ASR (SRM)	22M	224 ²	73.96 (↑ 0.65)
ResNet50	26M	224 ²	76.13
ResNet50+ASR (SE)	26M	224 ²	76.70 (↑ 0.57)
ResNet50+ASR (ECA)	26M	224 ²	76.87 (↑ 0.74)
ResNet50+ASR (SRM)	26M	224 ²	76.55 (↑ 0.42)
ResNet101	45M	224 ²	77.06
ResNet101+ASR (SE)	45M	224 ²	77.79 (↑ 0.73)
ResNet101+ASR (ECA)	45M	224 ²	77.63 (↑ 0.57)
ResNet101+ASR (SRM)	45M	224 ²	78.18 (↑ 1.12)
ViT-S	22M	224 ²	80.02
ViT-S+ASR (SE)	22M	224 ²	80.33 (↑ 0.31)
ViT-S+ASR (ECA)	22M	224 ²	80.37 (↑ 0.35)
ViT-S+ASR (SRM)	22M	224 ²	80.51 (↑ 0.49)
ViT-B	86M	224 ²	81.42
ViT-B+ASR (SE)	86M	224 ²	82.54 (↑ 1.12)
ViT-B+ASR (ECA)	86M	224 ²	82.38 (↑ 0.96)
ViT-B+ASR (SRM)	86M	224 ²	82.24 (↑ 0.82)
ViT-B	86M	384 ²	82.97
ViT-B+ASR (SE)	86M	384 ²	83.55 (↑ 0.58)
ViT-B+ASR (ECA)	86M	384 ²	83.86 (↑ 0.89)
ViT-B+ASR (SRM)	86M	384 ²	83.71 (↑ 0.74)

Table 2: Top-1 accuracy (%) of ASR on ImageNet-1k for models trained without any external data.

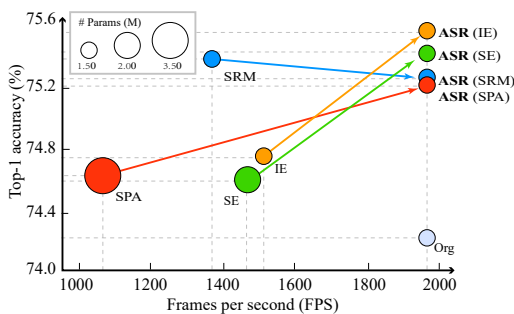


Figure 3: Top-1 accuracy, parameters size, and the inference speed of various attention modules and corresponding ASR.

Model		STL10	CIFAR100	CIFAR10
Resnet164	-	82.38	74.32	92.97
	ASR (SE)	83.70 (↑ 1.32)	75.36 (↑ 1.04)	94.47 (↑ 1.50)
	ASR (IE)	85.15 (↑ 2.77)	75.58 (↑ 1.26)	94.39 (↑ 1.42)
	ASR (SRM)	83.76 (↑ 1.38)	75.23 (↑ 0.91)	94.45 (↑ 1.48)
	ASR (SPA)	83.44 (↑ 1.06)	75.12 (↑ 0.80)	94.65 (↑ 1.68)
VGG19	-	79.23	72.48	93.15
	ASR (SE)	79.95 (↑ 0.72)	73.37 (↑ 0.89)	93.98 (↑ 0.83)
	ASR (IE)	80.48 (↑ 1.25)	73.41 (↑ 0.93)	93.55 (↑ 0.40)
	ASR (SRM)	80.35 (↑ 1.12)	73.33 (↑ 0.85)	93.60 (↑ 0.45)
	ASR (SPA)	80.23 (↑ 1.00)	73.38 (↑ 0.90)	93.79 (↑ 0.64)
ShuffleNetV2	-	80.34	71.12	91.68
	ASR (SE)	81.46 (↑ 1.12)	71.34 (↑ 0.22)	91.68 (↑ 0.00)
	ASR (IE)	82.83 (↑ 2.49)	71.89 (↑ 0.77)	91.90 (↑ 0.22)
	ASR (SRM)	81.28 (↑ 0.94)	71.79 (↑ 0.67)	91.69 (↑ 0.01)
	ASR (SPA)	82.15 (↑ 1.81)	72.05 (↑ 0.93)	91.71 (↑ 0.03)
MobileNet	-	80.35	66.87	90.97
	ASR (SE)	81.18 (↑ 0.83)	68.91 (↑ 2.04)	91.48 (↑ 0.51)
	ASR (IE)	81.38 (↑ 1.03)	69.45 (↑ 2.58)	91.30 (↑ 0.33)
	ASR (SRM)	81.51 (↑ 1.16)	69.04 (↑ 2.17)	91.09 (↑ 0.12)
	ASR (SPA)	81.35 (↑ 1.00)	68.56 (↑ 1.69)	91.36 (↑ 0.39)

Table 3: The accuracy (%) of ASR for various vision backbones on STL10, CIFAR100, and CIFAR10.

4 Experiments

Implementation details

In our study, we employ various backbone architectures, including vanilla ResNet (He et al. 2016), VGG (Simonyan and Zisserman 2014), ShuffleNetV2 (Ma et al. 2018), MobileNet (Howard et al. 2017), ViT (Dosovitskiy et al. 2020), RepVGG (Ding et al. 2021d), and ResNet-ACNet (Ding et al. 2019). Additionally, we use SE (Hu, Shen, and Sun 2018), IE (Wang et al. 2021; Liang et al. 2020), SRM (Lee, Kim, and Nam 2019), ECA (Wang et al. 2020), and SPA (Guo et al. 2020) as the attention modules in our experiments. We employ several popular datasets, namely ImageNet (Russakovsky et al. 2015), STL10 (Coates, Ng, and Lee 2011), and CIFAR10/100 (Krizhevsky, Hinton et al. 2009) in our experiments. Additionally, we use COCO (Lin et al. 2014) in our style transfer experiments. All experiments are performed using at least 3 runs to ensure statistical significance. We provide detailed recipes in the appendix.

ASR for various backbones

We examine the task of image classification to study the capability of ASR applied in popular visual backbones as shown in Table 2 and Table 3. Due to the consideration of a wide variety of backbone network structures, it’s hard to formulate them uniformly. See the appendix for specific details regarding ASR with each backbone.

Observations. Table 2 illustrates that ASR performs well on challenging datasets ImageNet, and is capable of enhancing the performance of popular transformer-based models ViT. The experimental results presented in Table 3 indicate that ASR is capable of significantly improving the performance of various backbone models on commonly used datasets, with the maximum improvement being 2.77% in terms of top-1 accuracy. It’s worth noting that we only choose classic attention modules as the training structure for SRP to showcase ASR’s effectiveness in our experiments.

However, in reality, ASR exhibits robust scalability and can be extended to incorporate diverse attention modules, having the potential for further enhancing model performance.

Additionally, as an attention-alike method, ASR exhibits performance differences from the original attention modules in terms of accuracy, frames per second (FPS), and parameter size as shown in Fig. 3. ASR has absolute advantages in terms of FPS and parameter size over attention modules. With an appropriate attention module, ASR can even outperform the attention modules in terms of accuracy for the reason that by learning constant attention that represents a learned average response, it is the potential to mitigate negative interference from the input and achieve better overall performance in an averaged sense. Overall, our experimental results suggest that ASR is a promising approach for enhancing the performance of various vision backbones.

The compatibility of ASR

ASR for existing attention modules. As shown in Fig. 1, ASR is an attention-like mechanism. It is natural to wonder whether ASR is compatible with DNNs that already incorporate attention modules. To investigate this, we conduct experiments as shown in Table 4, and find that ASR significantly improves the performance of DNNs that have attention modules.

Module κ		STL10		CIFAR100	
		w/o ASR	w/ ASR	w/o ASR	w ASR
ResNet83	SE	84.21	85.51 ($\uparrow 1.30$)	74.62	75.87 ($\uparrow 1.25$)
	IE	84.03	85.70 ($\uparrow 1.67$)	74.74	75.57 ($\uparrow 0.83$)
	SRM	82.09	84.83 ($\uparrow 2.74$)	75.38	75.78 ($\uparrow 0.40$)
	SPA	77.54 [‡]	80.88 ($\uparrow 3.34$)	74.64	74.92 ($\uparrow 0.28$)
ResNet164	SE	83.81	86.41 ($\uparrow 2.60$)	75.29	77.32 ($\uparrow 2.03$)
	IE	84.69	85.99 ($\uparrow 1.30$)	75.78	76.20 ($\uparrow 0.42$)
	SRM	84.85	85.20 ($\uparrow 0.35$)	75.32	77.18 ($\uparrow 1.86$)
	SPA	75.33 [‡]	79.61 ($\uparrow 4.28$)	75.48	77.25 ($\uparrow 1.77$)

Table 4: The experiments about the compatibility of ASR for existing attention modules. Given an attention module κ , ‘‘Without ASR’’ means the backbone with only the module κ . ‘‘With ASR’’ denotes the backbone with both κ and ASR (κ). [‡] We have repeated five runs for SPA on STL10. Although its performance is relatively low compared to other modules, it still demonstrates the effectiveness of ASR.

ASR for existing SRP methods. As a type of SRP, we also investigate the compatibility of ASR with other SRP methods. Specifically, we select RepVGG (Ding et al. 2021d) and ACNet (Ding et al. 2019), which utilize SRP in different ways and evaluated their performance with and without ASR (SE) as presented in Table 5. The results indicate that ASR is compatible with SRP and can further improve the performance of these models.

In conclusion, the experiments conducted in this section highlight that ASR, as a highly scalable SRP method, possesses the ability to not only improve the performance of visual backbone networks without any extra costs during inference but also to seamlessly integrate with homogeneous methods like attention modules and other SRP techniques.

Model	STL10	CIFAR100
RepVGGA0	83.48	68.80
RepVGGA0-ASR (SE)	84.01 ($\uparrow 0.53$)	69.38 ($\uparrow 0.58$)
RepVGGB3	87.05	76.70
RepVGGB3-ASR (SE)	88.29 ($\uparrow 1.24$)	77.42 ($\uparrow 0.72$)
ResNet56 [‡]	82.25	70.67
ResNet56-ACNet	83.11 ($\uparrow 0.86$)	71.42 ($\uparrow 0.75$)
ResNet56-ACNet-ASR (SE)	84.79 ($\uparrow 2.54$)	71.81 ($\uparrow 1.14$)
ResNet110 [‡]	82.02	72.60
ResNet110-ACNet	83.54 ($\uparrow 1.52$)	73.01 ($\uparrow 0.41$)
ResNet110-ACNet-ASR (SE)	86.13 ($\uparrow 4.11$)	73.46 ($\uparrow 0.86$)
ResNet164 [‡]	81.78	71.24
ResNet164-ACNet	83.91 ($\uparrow 2.13$)	71.60 ($\uparrow 0.36$)
ResNet164-ACNet-ASR (SE)	84.65 ($\uparrow 2.87$)	73.50 ($\uparrow 2.26$)

Table 5: Top-1 accuracy (%) of ASR (SE) applied to well-known SRP methods RepVGG (Ding et al. 2021d) and ACNet (Ding et al. 2019). RepVGGA0 and RepVGGB3 are RepVGG models with different layers of each stage and multipliers(Ding et al. 2021d). [‡] We follow the settings of ResNet in the official code of ACNet, which have different layers of each stage and design (basic-block) compared to the ResNet in Table 3.

5 Ablation study

(1) About multiple uses of ASR. Since ASR can eliminate the extra parameter and computation cost of the attention modules in the backbones during inference, theoretically, there will be no extra cost in the inference stage no matter how many times ASR is used for attention module re-parameterization. Therefore, we explore the optimal frequency denoted as δ of ASR on the model’s performance. As shown in Table 6, the performance of the model increases first and then decreases with the increase of δ . This phenomenon suggests that ASR can further enhance the performance of the network that has already been trained with ASR, but δ cannot be too large. This is because, in general, the output of the attention module goes through a Sigmoid activation function, whose each value is not large than 1. If δ is too large, the backbone network’s feature map will become small in value due to being multiplied by too many of these vectors, affecting the model’s training and information forwarding. Moreover, when δ is larger, the computational cost of training increases. Therefore, in all experiments in this paper, we generally choose $\delta = 1$.

Module	$\delta = 1$	$\delta = 2$	$\delta = 3$	$\delta = 4$
ASR (SE)	75.36	75.87	75.72	75.22
ASR (IE)	75.58	75.71	75.45	74.56
ASR (SRM)	<u>75.23</u>	75.45	75.61	75.11
ASR (SPA)	75.12	75.43	75.81	75.62

Table 6: Top-1 accuracy (%) of ResNet164 with different numbers δ of ASR inserted at the same position on CIFAR100. Bold and underline indicate the best results and the second best results, respectively.

(2) About the learnable input ψ . We discuss the importance of the learnable input ψ for ASR. From the ASR paradigm, we verify the performance when ψ is a unlearnable constant C_i or N_i , where C_i means that the all elements

of ψ are constant i and N_i means that ψ samples from the normal distribution $N(\mathbf{0}, i^2 \mathbf{I}_{\dim(\psi)})$. The results are shown in Table 7, where we can find the performance with constant ψ is weaker relative to the learnable one, while the performance seems good when $C_{0.1}$. Therefore, in the experiments of this paper ϕ are initialized with $C_{0.1}$, and results about other initializations can be found in the Appendix.

Module	Ours	$C_{0.1}$	$C_{0.3}$	$C_{0.5}$	$N_{0.1}$	$N_{0.3}$	$N_{0.5}$
ASR (SE)	75.36	75.18	75.09	75.07	74.56	75.02	74.93
ASR (IE)	75.58	75.24	75.11	75.14	75.36	75.17	75.47

Table 7: ResNet164-ASR without learnable input ψ on CIFAR100. C_i and N_i denote the initialization of unlearnable ψ . C_i means that the all elements of ψ are constant i and N_i means that ψ samples from the normal distribution $N(\mathbf{0}, i^2 \mathbf{I}_{\dim(\psi)})$.

6 Analysis

(1) Why do attention values approach some constant vectors? In the introduction, we observe *Stripe Observation* consistently across a wide range of experimental settings. This phenomenon is intriguing and although not easily explained by theory, it appears empirically reasonable. Given a dataset D , certain priors such as location and color priors exist in D and they have a significant impact on neural network learning, especially for attention networks that excel at capturing inductive biases. The attention mechanism adaptively adjusts the weights of feature maps to extract key information and suppress irrelevant information, which can be visualized through Grad-CAM (Selvaraju et al. 2017). Specifically, we use the pre-trained SENet (Hu, Shen, and Sun 2018) and SRMNet (Lee, Kim, and Nam 2019) as backbones and randomly sample 500 images from the STL10 and ImageNet datasets, and measure the average attention visualizations (using Grad-CAM) of these images under the given backbones, as shown in Fig. 4. We find that the regions of interest identified by the network tend to be biased toward the center of the images in all visualizations. This is because in the shooting or annotation process of these datasets, the target object y was inherently present in the salient location of the image (close to the center), or else the image would not be labeled with the corresponding label of y . Therefore, intuitively, the existence of a series of constant ‘‘attention’’ values that satisfy certain priors of the network is reasonable, and these constant vectors can be regarded as the average embodiment of certain priors in D .

Moreover, despite the fact that according to the *Stripe Observation*, attention values approach to some constant vectors, if we directly replace the attention module with these vectors during the inference phase, taking Table 3 as a baseline, the average performance will decrease by approximately 28%, and there will still be around 15% performance loss even with finetuning. Therefore, our proposed ASR still needs to consider the participation of the attention module during training.

(2) Why does ASR work? ASR generates constant vectors through the attention module to help the training of DNNs,

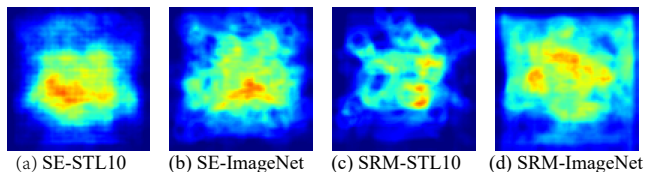


Figure 4: The visualization of average Grad-CAM.

and we find that these constant vectors from ASR can regulate the noise to enhance the robustness of DNNs and help model training.

Theorem 6.1. Consider ASR for a L layers residual neural network with attention module $T(\cdot)$, and the corresponding constant input at t -th layer ψ_t , i.e., $x_{t+1} = x_t + f(x_t; W_t) \odot T[f(\psi_t)]$, $t = 0, 1, \dots, L - 1$. Let ϵ be the perturbation from the noise and satisfies $\|x_0^\epsilon - x_0\| = \epsilon$, and $\epsilon_t = \|x_t^\epsilon - x_t\|$, we have

$$\epsilon_{t+1} \leq \epsilon_t (1 + \alpha_t \|W_t\|_2), \quad (8)$$

where $\alpha_t = \max\{T[f(\psi_t)]\}$ and \max refers to the largest element in a vector. See proof in the appendix.

Given an input x_0 of the network and a perturbation ϵ , let the noise input x_0^ϵ satisfy $x_0^\epsilon \in \{x \mid \|x - x_0\| = \epsilon\}$. According to Theorem 6.1, for a L layers ResNet, the noise impact $\epsilon_L = \|x_L^\epsilon - x_L\|$ satisfies the following inequation:

$$\epsilon_L \leq \epsilon_{L-1} (1 + \alpha_t \|W_{L-1}\|_2) \leq \epsilon M, \quad (9)$$

where $M = \prod_{t=1}^{L-1} (1 + \alpha_t \|W_t\|_2)$ and it will be a constant in inference phase. Without ASR, i.e., $\alpha_t = 1$, the upper bound of the noise impact ϵ_L increases rapidly with the network depth L due to $(1 + \alpha_t \|W_{L-1}\|_2) \geq 1$. However, with the regulation of ASR, which restricts $0 \leq \alpha_t \leq 1$, this increasing trend of the upper bound can be mitigated, resulting in a robust model. Moreover, since mild noise is generally beneficial to model training, ASR needs to adaptively allow for a moderate amount of noise during training. Additionally, the constant vectors $T[f(\psi_t)]$ generated by ASR cannot be zero vectors, as this would lead to the degradation of the residual network to $x_{t+1} = x_t$, although the upper bound of noise impact ϵ_L could be minimized.

We conduct experiments on three types of noise attacks to empirically verify the ability of ASR in regulating noise to improve model robustness, including batch noise, constant noise, and random noise. We consider the style transfer task, which generally adopts the instance normalization (IN) without batch noise, rather than BN, as adding batch noise would significantly reduce the quality of generated images due to noise interference. As shown in Fig. 5, ASR can significantly alleviate the adverse effects of noise when batch noise is introduced, resulting in image quality comparable to that of IN without batch noise.

Next, we examine constant noise and random noise attacks, following the settings in (Liang et al. 2020), we inject noise N_a and N_b in each BN layer of ResNet164, i.e., $\text{BN}(\mathbf{x}; \gamma, \beta) = [\frac{x - \mu}{\sigma} \odot N_a + N_b] \odot \gamma + \beta$. For constant noise, N_a and N_b are constant, while $N_a \sim N(1, \sigma_{N_a})$ and $N_b \sim N(0, \sigma_{N_b})$ in random noise scenario. As shown in Table 8, both types of noise have a large impact on neural network training. However, compared with the original network, ASR can significantly mitigate the performance loss

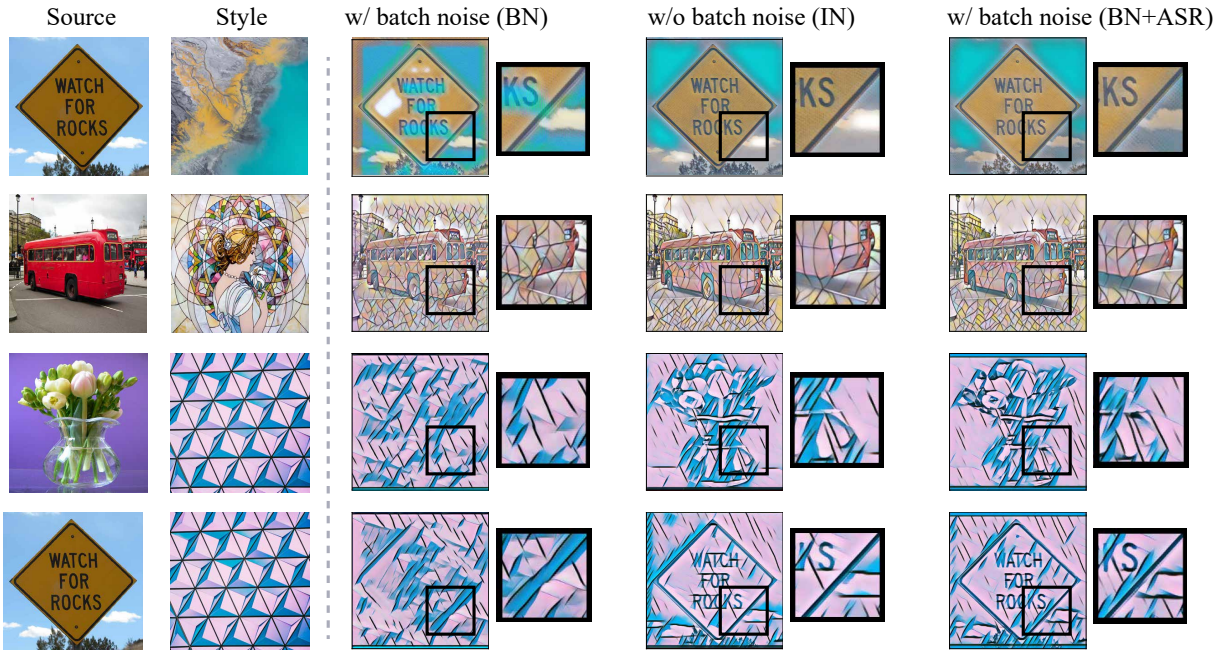


Figure 5: The results about the batch noise attack. Zoom in for best view. See appendix for more results.

(N_a, N_b)	Origin	ASR (SE)	ASR (IE)	ASR (SRM)
(1.0,0.0)	74.32	75.36 ($\uparrow 1.04$)	75.58 ($\uparrow 1.26$)	75.23 ($\uparrow 0.91$)
(0.8,0.8)	45.42	68.81 ($\uparrow 23.39$)	69.85 ($\uparrow 24.43$)	69.57 ($\uparrow 24.15$)
(0.8,0.5)	46.10	71.13 ($\uparrow 25.03$)	72.38 ($\uparrow 26.28$)	71.69 ($\uparrow 25.59$)
(0.5,0.5)	35.77	72.18 ($\uparrow 36.41$)	72.69 ($\uparrow 36.92$)	71.85 ($\uparrow 36.08$)
(0.5,0.2)	73.10	74.48 ($\uparrow 1.38$)	75.36 ($\uparrow 2.26$)	75.02 ($\uparrow 1.92$)
$(\sigma_{N_a}, \sigma_{N_b})$	Origin	ASR (SE)	ASR (IE)	ASR (SRM)
(0.1,0.1)	73.16 \pm 0.26	75.29 \pm 0.13	75.00 \pm 0.79	75.00 \pm 0.12
(0.1,0.2)	73.75 \pm 0.47	74.91 \pm 0.24	74.98 \pm 0.10	75.04 \pm 0.23
(0.2,0.1)	72.63 \pm 0.49	75.15 \pm 0.19	74.85 \pm 0.06	75.22 \pm 0.11
(0.2,0.2)	72.87 \pm 0.29	75.07 \pm 0.14	75.47 \pm 0.15	75.02 \pm 0.23
(0.3,0.3)	73.40 \pm 0.59	75.33 \pm 0.12	74.76 \pm 0.09	75.24 \pm 0.36

Table 8: Top-1 Accuracy (%) of vanilla ResNet164 (**Origin**) and ASR-enhanced ResNet164 on CIFAR100 under constant or random noise attack. σ refers to the variance of the normal distribution used to generate random noise.

suffered by the model, and the performance is more stable, i.e., the variance of top-1 accuracy is smaller.

(3) How to make ASR stronger? Firstly, the attention module in ASR is crucial for performance improvement. We can remove the attention module and only retain a learnable vector as a constant vector needed for ASR inference. The experimental results, as shown in Table 9, indicate that although this approach also leads to some performance improvement, its effectiveness is significantly lower than that of ASR with specific attention modules. Additionally, in the experiments presented in this paper, we find that the performance of ASR is closely related to the selection of attention modules, and different modules exhibit varying performance improvements in various tasks. For instance, as shown in Table 3, for ResNet164, the IE module shows a significant performance advantage, while in ViT, the SE module performs best. These observations imply that the specific modules need to be designed for different scenarios. Since all of ASR can be integrated into the backbone during the in-

ference phase, researchers can consider more complex and efficient attention modules in the ASR paradigm to meet the needs of different tasks without worrying about the additional parameter load and inference cost generated by the module during inference.

Attention module	STL10	CIFAR100	CIFAR10
-	82.38	74.32	92.97
\times	83.44 ($\uparrow 1.06$)	74.46 ($\uparrow 0.14$)	92.84 ($\downarrow -0.13$)
\checkmark	85.15 ($\uparrow 2.77$)	75.58 ($\uparrow 1.26$)	94.65 ($\uparrow 1.68$)

Table 9: ResNet164-ASR with or without attention modules.

(4) Limitation of proposed ASR. ASR is inspired by the intriguing *Stripe Observation*, which reveals that the channel attention values corresponding to any input in the dataset approach to some constant vectors after neural network training. However, this observation does not hold for other types of attention, including spatial attention and transformer-based attention (see appendix for visualization). These types of attention have individual attention maps for different inputs, which means that ASR may not be directly transferable to their corresponding attention modules. Further details and comparisons can be found in the appendix. Additionally, from an application perspective, although ASR has been validated in multiple classification scenarios, its versatility for other more challenging downstream tasks remains uncertain. Fortunately, in Analysis (3) we suggest that the researchers can design more complex and tailored attention modules to solve these tasks benefiting from the flexibility of the ASR paradigm.

7 Conclusion

In this paper, we introduce a novel attention-alike structural re-parameterization (ASR) method, tailored for the channel attention mechanism, which enables effective interconver-

sion between different network architectures. Our discovery of the *Stripe Observation* provides new insights into the channel attention mechanism from a statistical perspective, leading to the development of ASR. Extensive experiments demonstrate that ASR can improve model performance without extra parameters and inference time. We have also provided experimental and theoretical evidence for the compatibility, effectiveness, and robustness of ASR, making it a promising approach for practical applications.

References

- Cao, J.; Li, Y.; Sun, M.; Chen, Y.; Lischinski, D.; Cohen-Or, D.; Chen, B.; and Tu, C. 2020. Do-conv: Depthwise over-parameterized convolutional layer. *arXiv 2006.12030*.
- Cao, Y.; Xu, J.; Lin, S.; Wei, F.; and Hu, H. 2019. Gcnet: Non-local networks meet squeeze-excitation networks and beyond. In *IEEE Conf. Comput. Vis. Worksh.*, 0–0.
- Chen, S.; Chen, Y.; Yan, S.; and Feng, J. 2019. Efficient differentiable Neural Architecture Search with Meta Kernels. *arXiv 1912.04749*.
- Coates, A.; Ng, A.; and Lee, H. 2011. An analysis of single-layer networks in unsupervised feature learning. In *Proceedings of the fourteenth international conference on artificial intelligence and statistics*, 215–223. JMLR Workshop and Conference Proceedings.
- Ding, X.; Guo, Y.; Ding, G.; and Han, J. 2019. Acnet: Strengthening the kernel skeletons for powerful cnn via asymmetric convolution blocks. In *Proceedings of the IEEE/CVF international conference on computer vision*, 1911–1920.
- Ding, X.; Hao, T.; Tan, J.; Liu, J.; Han, J.; Guo, Y.; and Ding, G. 2021a. Lossless cnn channel pruning via decoupling remembering and forgetting. In *ICCV*.
- Ding, X.; Xia, C.; Zhang, X.; Chu, X.; Han, J.; and Ding, G. 2021b. Repmlp: Re-parameterizing convolutions into fully-connected layers for image recognition. *arXiv preprint arXiv:2105.01883*.
- Ding, X.; Zhang, X.; Han, J.; and Ding, G. 2021c. Diverse branch block: Building a convolution as an inception-like unit. In *Proceedings of the IEEE/CVF Conference on Computer Vision and Pattern Recognition*, 10886–10895.
- Ding, X.; Zhang, X.; Ma, N.; Han, J.; Ding, G.; and Sun, J. 2021d. Repvgg: Making vgg-style convnets great again. In *Proceedings of the IEEE/CVF conference on computer vision and pattern recognition*, 13733–13742.
- Dosovitskiy, A.; Beyer, L.; Kolesnikov, A.; Weissborn, D.; Zhai, X.; Unterthiner, T.; Dehghani, M.; Minderer, M.; Heigold, G.; Gelly, S.; et al. 2020. An image is worth 16x16 words: Transformers for image recognition at scale. *arXiv preprint arXiv:2010.11929*.
- Fu, J.; Liu, J.; Tian, H.; Li, Y.; Bao, Y.; Fang, Z.; and Lu, H. 2019. Dual attention network for scene segmentation. In *IEEE Conf. Comput. Vis. Pattern Recog.*, 3146–3154.
- Gao, S.; Zheng, C.; Zhang, X.; Liu, S.; Wu, B.; Lu, K.; Zhang, D.; and Wang, N. 2023. RCBSR: re-parameterization convolution block for super-resolution. In *Computer Vision–ECCV 2022 Workshops: Tel Aviv, Israel, October 23–27, 2022, Proceedings, Part II*, 540–548. Springer.
- Gao, Z.; Xie, J.; Wang, Q.; and Li, P. 2019. Global second-order pooling convolutional networks. In *IEEE Conf. Comput. Vis. Pattern Recog.*, 3024–3033.
- Guo, J.; Ma, X.; Sansom, A.; McGuire, M.; Kalaani, A.; Chen, Q.; Tang, S.; Yang, Q.; and Fu, S. 2020. Spanet: Spatial pyramid attention network for enhanced image recognition. In *2020 IEEE International Conference on Multimedia and Expo (ICME)*, 1–6. IEEE.
- Guo, S.; Alvarze, J. M.; and Salzmann, M. 2020. Expandnets: linear over re-parameterization to train compact convolutional networks. In *NeurIPS*.
- He, K.; Zhang, X.; Ren, S.; and Sun, J. 2016. Deep residual learning for image recognition. In *IEEE Conf. Comput. Vis. Pattern Recog.*, 770–778.
- Hou, Q.; Zhou, D.; and Feng, J. 2021. Coordinate Attention for Efficient Mobile Network Design. *arXiv preprint arXiv:2103.02907*.
- Howard, A. G.; Zhu, M.; Chen, B.; Kalenichenko, D.; Wang, W.; Weyand, T.; Andreetto, M.; and Adam, H. 2017. Mobilenets: Efficient convolutional neural networks for mobile vision applications. *arXiv preprint arXiv:1704.04861*.
- Hu, J.; Shen, L.; and Sun, G. 2018. Squeeze-and-excitation networks. In *IEEE Conf. Comput. Vis. Pattern Recog.*, 7132–7141.
- Hu, M.; Feng, J.; Hua, J.; Lai, B.; Huang, J.; Gong, X.; and Hua, X.-S. 2022. Online convolutional re-parameterization. In *Proceedings of the IEEE/CVF Conference on Computer Vision and Pattern Recognition*, 568–577.
- Huang, T.; You, S.; Zhang, B.; Du, Y.; Wang, F.; Qian, C.; and Xu, C. 2022. Dyrep: Bootstrapping training with dynamic re-parameterization. In *Proceedings of the IEEE/CVF Conference on Computer Vision and Pattern Recognition*, 588–597.
- Huang, Z.; Liang, M.; and Lin, L. 2023. On Robust Numerical Solver for ODE via Self-Attention Mechanism. *arXiv preprint arXiv:2302.10184*.
- Huang, Z.; Liang, S.; Liang, M.; and Yang, H. 2020. DI-ANet: Dense-and-Implicit Attention Network. In *AAAI*, 4206–4214.
- Ioffe, S.; and Szegedy, C. 2015. Batch normalization: Accelerating deep network training by reducing internal covariate shift. In *International conference on machine learning*, 448–456. pmlr.
- Krizhevsky, A.; Hinton, G.; et al. 2009. Learning multiple layers of features from tiny images.
- Lee, H.; Kim, H.-E.; and Nam, H. 2019. Srm: A style-based recalibration module for convolutional neural networks. In *Int. Conf. Comput. Vis.*, 1854–1862.
- Liang, S.; Huang, Z.; Liang, M.; and Yang, H. 2020. Instance enhancement batch normalization: An adaptive regulator of batch noise. In *Proceedings of the AAAI Conference on Artificial Intelligence*, volume 34, 4819–4827.

- Lin, T.-Y.; Maire, M.; Belongie, S.; Hays, J.; Perona, P.; Ramanan, D.; Dollár, P.; and Zitnick, C. L. 2014. Microsoft coco: Common objects in context. In *Eur. Conf. Comput. Vis.*, 740–755.
- Luo, J.; Si, W.; and Deng, Z. 2022. Few-Shot Learning for Radar Signal Recognition Based on Tensor Imprint and Re-Parameterization Multi-Channel Multi-Branch Model. *IEEE Signal Processing Letters*, 29: 1327–1331.
- Ma, N.; Zhang, X.; Zheng, H.-T.; and Sun, J. 2018. Shufflenet v2: Practical guidelines for efficient cnn architecture design. In *Proceedings of the European conference on computer vision (ECCV)*, 116–131.
- Qin, Z.; Zhang, P.; Wu, F.; and Li, X. 2021. Fcanet: Frequency channel attention networks. In *Proceedings of the IEEE/CVF international conference on computer vision*, 783–792.
- Russakovsky, O.; Deng, J.; Su, H.; Krause, J.; Satheesh, S.; Ma, S.; Huang, Z.; Karpathy, A.; Khosla, A.; Bernstein, M.; et al. 2015. Imagenet large scale visual recognition challenge. *International journal of computer vision*, 115(3): 211–252.
- Selvaraju, R. R.; Cogswell, M.; Das, A.; Vedantam, R.; Parikh, D.; and Batra, D. 2017. Grad-CAM: Visual Explanations from Deep Networks via Gradient-Based Localization. In *International Conference on Computer Vision*.
- Simonyan, K.; and Zisserman, A. 2014. Very deep convolutional networks for large-scale image recognition. *arXiv preprint arXiv:1409.1556*.
- Touvron, H.; Bojanowski, P.; Caron, M.; Cord, M.; El-Nouby, A.; Grave, E.; Izacard, G.; Joulin, A.; Synnaeve, G.; Verbeek, J.; et al. 2022. Resmlp: Feedforward networks for image classification with data-efficient training. *IEEE Transactions on Pattern Analysis and Machine Intelligence*.
- Ulyanov, D.; Vedaldi, A.; and Lempitsky, V. 2016. Instance normalization: The missing ingredient for fast stylization. *arXiv preprint arXiv:1607.08022*.
- Vaswani, A.; Shazeer, N.; Parmar, N.; Uszkoreit, J.; Jones, L.; Gomez, A. N.; Kaiser, Ł.; and Polosukhin, I. 2017. Attention is all you need. In *Adv. Neural Inform. Process. Syst.*, 5998–6008.
- Wang, J.; Chen, Y.; Yu, S. X.; Cheung, B.; and LeCun, Y. 2021. Recurrent Parameter Generators. *arXiv preprint arXiv:2107.07110*.
- Wang, Q.; Wu, B.; Zhu, P.; Li, P.; Zuo, W.; and Hu, Q. 2020. ECA-net: Efficient channel attention for deep convolutional neural networks. In *IEEE Conf. Comput. Vis. Pattern Recog.*, 11534–11542.
- Wang, X.; Dong, C.; and Shan, Y. 2022. Reprs: Training efficient vgg-style super-resolution networks with structural re-parameterization and batch normalization. In *Proceedings of the 30th ACM International Conference on Multimedia*, 2556–2564.
- Woo, S.; Park, J.; Lee, J.-Y.; and So Kweon, I. 2018. Cbam: Convolutional block attention module. In *Eur. Conf. Comput. Vis.*, 3–19.
- Wu, Y.; and He, K. 2018. Group normalization. In *Proceedings of the European conference on computer vision (ECCV)*, 3–19.
- Yang, Y.; Wu, J.; Li, H.; Li, X.; Shen, T.; and Lin, Z. 2020. Dynamical system inspired adaptive time stepping controller for residual network families. In *Proceedings of the AAAI Conference on Artificial Intelligence*, volume 34, 6648–6655.
- Yu, W.; Luo, M.; Zhou, P.; Si, C.; Zhou, Y.; Wang, X.; Feng, J.; and Yan, S. 2022. Metaformer is actually what you need for vision. In *Proceedings of the IEEE/CVF conference on computer vision and pattern recognition*, 10819–10829.
- Zhang, H.; Wu, C.; Zhang, Z.; Zhu, Y.; Zhang, Z.; Lin, H.; Sun, Y.; He, T.; Mueller, J.; Manmatha, R.; et al. 2020. Resnest: Split-attention networks. *arXiv preprint arXiv:2004.08955*.
- Zhang, M.; Yu, X.; Rong, J.; and Ou, L. 2021. Repnas: Searching for efficient re-parameterizing blocks. *arXiv 2109.03508*.
- Zhang, R.; Wei, J.; Lu, W.; Zhang, L.; Ji, Y.; Xu, J.; and Lu, X. 2022. CS-REP: Making Speaker Verification Networks Embracing Re-Parameterization. In *ICASSP 2022-2022 IEEE International Conference on Acoustics, Speech and Signal Processing (ICASSP)*, 7082–7086. IEEE.
- Zhong, S.; Wen, W.; and Qin, J. 2022. Mix-Pooling Strategy for Attention Mechanism. *arXiv preprint arXiv:2208.10322*.
- Zhou, H.; Liu, L.; Zhang, H.; He, H.; and Zheng, N. 2022. CMB: A Novel Structural Re-parameterization Block without Extra Training Parameters. In *2022 International Joint Conference on Neural Networks (IJCNN)*, 1–9. IEEE.
- Zhu, X.; Cheng, D.; Zhang, Z.; Lin, S.; and Dai, J. 2019. An empirical study of spatial attention mechanisms in deep networks. In *Int. Conf. Comput. Vis.*, 6688–6697.

A The Proof of Theorem 6.1

Theorem 6.1 Consider ASR for a L layers residual neural network with attention module $T(\cdot)$, and the corresponding constant input at t -th layer ψ_t , i.e., $x_{t+1} = x_t + f(x_t; W_t) \odot T[f(\psi_t)]$, $t = 0, 1, \dots, L - 1$. Let ϵ be the perturbation from the noise and satisfies $\|x_0^\epsilon - x_0\| = \epsilon$, and $\epsilon_t = \|x_t^\epsilon - x_t\|$, we have

$$\epsilon_{t+1} \leq \epsilon_t (1 + \alpha_t \|W_t\|_2), \quad (10)$$

where $\alpha_t = \max\{T[f(\psi_t)]\}$ and \max refers to the largest element in a vector. See proof in the appendix.

Proof. Let $H(x) = f(x; W_t) \odot T[f(\psi_t)]$, according to Taylor expansion, we have

$$H(x_t^\epsilon) = H(x_t) + (x_t^\epsilon - x_t)^T \nabla_x H(x)|_{x=x_t} \quad (11)$$

For $\epsilon_{t+1} = \|x_{t+1}^\epsilon - x_{t+1}\|$, we have

$$\begin{aligned} \epsilon_{t+1} &= \|x_{t+1}^\epsilon - x_{t+1}\| \\ &= \|x_t^\epsilon + f(x_t^\epsilon; W_t) \odot T[f(\psi_t)] - x_t - f(x_t; W_t) \odot T[f(\psi_t)]\| \\ &= \|(x_t^\epsilon - x_t) + f(x_t^\epsilon; W_t) \odot T[f(\psi_t)] - f(x_t; W_t) \odot T[f(\psi_t)]\| \\ &= \|(x_t^\epsilon - x_t) + (x_t^\epsilon - x_t)^T \nabla_x H(x)|_{x=x_t}\| && \text{Since Eq.(11)} \\ &\leq \|(x_t^\epsilon - x_t)\| \cdot (1 + \|\nabla_x H(x)|_{x=x_t}\|) && \text{Since } \|ab\| \leq \|a\| \|b\| \\ &= \epsilon_t (1 + \|\nabla_x H(x)|_{x=x_t}\|) \end{aligned}$$

Next, we analyze $\nabla_x H(x)|_{x=x_t}$. We also follow and consider the assumption (Yang et al. 2020; Huang, Liang, and Lin 2023) that $f(x_t; W_t)$ is consists of linear transformation and ReLU non-linear activation \mathbf{A} , i.e., $f(x_t; W_t) = \mathbf{A}W_t x_t$. Note that \mathbf{A} is a diagonal matrix

$$\mathbf{A} = \text{diag}(a_1, a_2, \dots, a_d), \quad a_1, a_2, \dots, a_d \in \{0, 1\}, \quad (12)$$

where d is dimension of x_t and each element $a_i, i = 1, 2, \dots, d$ in \mathbf{A} is 0 or 1. If the i^{th} element in x_t is positive, the value of $a_i = 1$, otherwise equals to zero. Therefore the 2-norm, i.e., the largest singular value, of \mathbf{A} is less than 1, i.e.,

$$\|\mathbf{A}\|_2 = \sqrt{\lambda_{\max} \mathbf{A}^T \mathbf{A}} = \sqrt{\lambda_{\max} \mathbf{A}} \leq 1 \quad (13)$$

Hence, we can further estimate $\|\nabla_x H(x)|_{x=x_t}\|$ that

$$\begin{aligned} \|\nabla_x H(x)|_{x=x_t}\| &= \|\nabla_x f(x; W_t)|_{x=x_t} \odot T[f(\psi_t)] + f(x_t; W_t) \odot \nabla_x T[f(\psi_t)]\| \\ &\leq \|\mathbf{A}W_t \mathbf{I} \odot T[f(\psi_t)]\| + 0 \\ &\leq \alpha_t \cdot \|\mathbf{A}\| \|W_t\| \\ &\leq \alpha_t \|W_t\| && \text{Since Eq.(13)} \end{aligned}$$

Therefore, we have $\epsilon_{t+1} \leq \epsilon_t (1 + \alpha_t \|W_t\|_2)$. □

B ASR for different neural network layers in inference phase

In the main text, we find that the ‘‘attention values’’ $\mathbf{v}_{\psi, \theta}$ generated by ASR are some constant vector, for the various common-used modules $\mathbf{B}_{\hat{\theta}}$ in the backbone, we can seamlessly find the corresponding transformation g such that

$$\mathbf{B}_{\hat{\theta}} \odot \mathbf{v}_{\psi, \theta} = \mathbf{B}_{g[\hat{\theta}, \psi, \theta]}, \quad (14)$$

(1) For the convolutional layer, if $\mathbf{B}_{\hat{\theta}}$ is a convolutional layer \mathcal{C} with kernels \mathbf{K} and bias \mathbf{b} , then we have

$$\begin{aligned} \mathcal{C}(\mathbf{x}; \mathbf{K}, \mathbf{b}) \odot \mathbf{v}_{\psi, \theta} &= (\mathbf{x} * \mathbf{K}) \odot \mathbf{v}_{\psi, \theta} + \mathbf{b} \odot \mathbf{v}_{\psi, \theta} \\ &= \mathbf{x} * (\mathbf{K} \odot \mathbf{v}_{\psi, \theta}) + \mathbf{b} \odot \mathbf{v}_{\psi, \theta} \\ &= \mathcal{C}(\mathbf{x}; \mathbf{K} \odot \mathbf{v}_{\psi, \theta}, \mathbf{b} \odot \mathbf{v}_{\psi, \theta}), \\ &\equiv \mathcal{C}(\mathbf{x}; \mathbf{K}', \mathbf{b}') \end{aligned} \quad (15)$$

where $*$ denote convolution and $\mathbf{K} \odot \mathbf{v}_{\psi, \theta}$ means that the the product of i -th elements of $\mathbf{v}_{\psi, \theta}$ and i -th kernel of \mathbf{K} . Since the existing SRP methods mainly merge various neural network layers into a convolutional layer, therefore ASR is compatible with most of these SRP methods.

(2) For the normalization layer κ , like batch normalization (Ulyanov, Vedaldi, and Lempitsky 2016), instance normalization (Ioffe and Szegedy 2015), group normalization (Wu and He 2018), etc., they generally can be formulated as

$$\kappa(x; \mu, \sigma, \gamma, \beta) = \frac{x - \mu}{\sigma} \odot \gamma + \beta, \quad (16)$$

where $\mu, \sigma, \gamma, \beta$ are the parameters of each kind of normalization method. For ASR, the Eq.(14) can be rewritten as

$$\begin{aligned} \kappa(\mathbf{x}; \mu, \sigma, \gamma, \beta) \odot \mathbf{v}_{\psi, \theta} &= \frac{(\mathbf{x} - \mu) \odot \gamma \odot \mathbf{v}_{\psi, \theta}}{\sigma} + \beta \odot \mathbf{v}_{\psi, \theta} \\ &= \kappa(\mathbf{x}; \gamma \odot \mathbf{v}_{\psi, \theta}, \beta \odot \mathbf{v}_{\psi, \theta}), \\ &\equiv \kappa(\mathbf{x}; \mu, \sigma, \gamma', \beta') \end{aligned} \quad (17)$$

(3) For the fully connected layer $f(x) = Wx$, we have

$$\begin{aligned} f(x) \odot \mathbf{v}_{\psi, \theta} &= Wx \odot \mathbf{v}_{\psi, \theta} \\ &= (W \odot \mathbf{v}_{\psi, \theta})x \equiv W'x \end{aligned} \quad (18)$$

(4) For the transformer-based attention layer T , we have

$$\begin{aligned} T(x; W_Q, W_K, W_V) \odot \mathbf{v}_{\psi, \theta} &= \frac{W_Q x (W_K x)^T}{\sqrt{d_k}} W_V x \odot \mathbf{v}_{\psi, \theta} \\ &= \frac{W_Q x (W_K x)^T}{\sqrt{d_k}} (W_V \odot \mathbf{v}_{\psi, \theta}) x \\ &\equiv \frac{W_Q x (W_K x)^T}{\sqrt{d_k}} W'_V x \\ &= T(x; W_Q, W_K, W'_V) \end{aligned} \quad \text{Since Eq.(18)}$$

C Introduction of implementation details

In Section C, we present the experimental details, followed by an explanation in Section C on how ASR is incorporated into various backbones.

Experiment details

Unless otherwise specified, we follow the settings of (He et al. 2016; Simonyan and Zisserman 2014; Ding et al. 2021d; Ma et al. 2018; Howard et al. 2017; Ding et al. 2019). Specifically, all models using STL10, CIFAR10, and CIFAR100 datasets with epoch set to 164. During training, we apply standard data augmentation techniques such as normalization, random cropping, and horizontal flipping. The batch size of CIFAR10, CIFAR100, and STL10 is 128, 128, 16, respectively. The other hyperparameter settings of CIFAR10, CIFAR100, STL10 and ImageNet are shown in Table 10 and Table 11 respectively. The patch size of ViT is 16.

	ResNet83	ResNet164	VGG19	ShuffleNetV2	MobileNet	RepVGG	ResNet-ACNet
optimizer	SGD (0.9)	SGD (0.9)	SGD (0.9)	SGD (0.9)	SGD (0.9)	SGD (0.9)	SGD (0.9)
schedule	81/122	81/122	60/120/160	60/120/160	60/120/160	130	cosine annealing
weight decay	1.00E-04	1.00E-04	5.00E-04	5.00E-04	5.00E-04	1.00E-04	1.00E-04
gamma	0.1	0.1	0.2	0.2	0.2	0.1	0.333
lr	0.1	0.1	0.1	0.1	0.1	0.1	0.1

Table 10: Implementation details for **CIFAR10/100, STL10** image classification. Normalization and standard data augmentation (random cropping and horizontal flipping) are applied to the training data.

	ResNet34	ResNet50	ResNet101	ViT-S	ViT-B	ViT-B \uparrow 384
optimizer	SGD (0.9)	SGD (0.9)	SGD (0.9)	AdamW	AdamW	AdamW
schedule	30/60/90	30/60/90	30/60/90	cosine annealing	cosine annealing	cosine annealing
weight decay	1.00E-04	1.00E-04	1.00E-04	5.00E-02	5.00E-02	1.00E-08
gamma	0.1	0.1	0.1	-	-	-
lr	0.1	0.1	0.1	5.00E-04	5.00E-04	5.00E-06
epoch	100	100	100	300	300	30
batch size	128	128	128	256	256	64

Table 11: Implementation details for **ImageNet 2012** image classification. Normalization and standard data augmentation (random cropping and horizontal flipping) are applied to the training data. The random cropping of size 224 by 224 is used in these experiments.

Name	Explanation
optimizer	Optimizer
depth	The depth of the network
schedule	Decrease learning rate at these epochs
wd	Weight decay
gamma	The multiplicative factor of learning rate decay
lr	Initial learning rate

Table 12: The additional explanation.

Application details

In this section, we provide detailed information on how we apply ASR to different architectures during the training phase. We focus on ResNet and ResNet-ACNet, VGG and RepVGG, ShuffleNetV2, MobileNet, and ViT. For each architecture, we specify the location of ASR within the block and provide a visualization to facilitate understanding. Normally, the placement of ASR is typically situated post the individual layers within the model architecture. Specifically, it is conventionally positioned subsequent to batch normalization and prior to the integration of residual connections and ReLU. In essence, ASR plays the role of calibration for the outputs of each stratum within the model architecture.

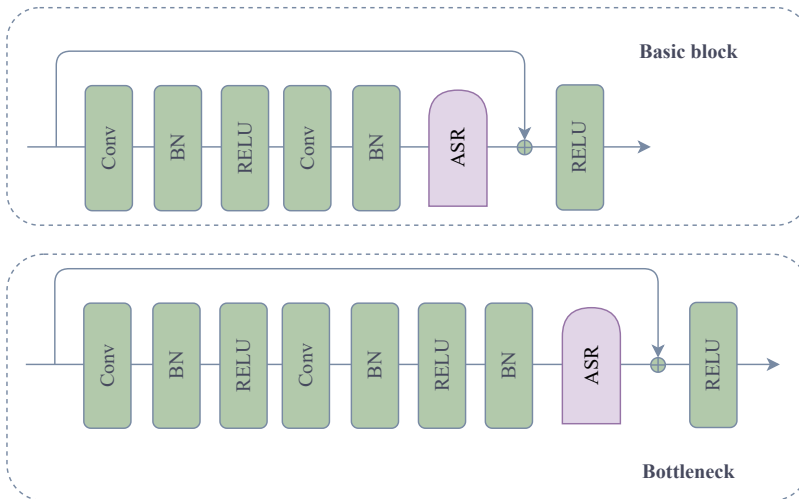


Figure 6: ASR in the blocks of ResNet during the training phase.

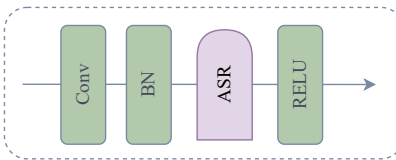


Figure 7: ASR in the block of VGG during the training phase.

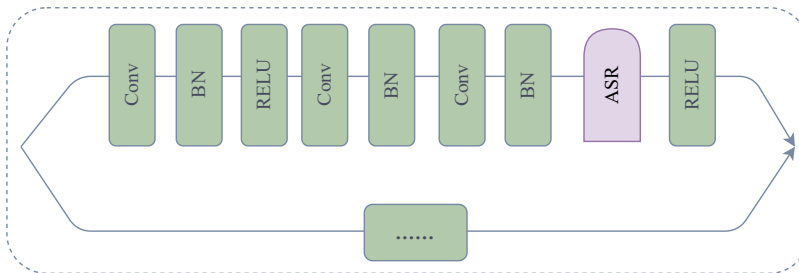


Figure 8: ASR in the block of ShuffleNetV2 during the training phase.

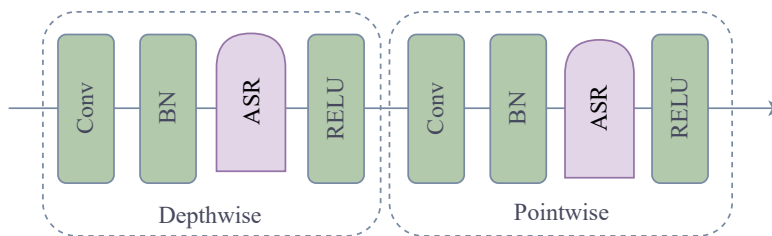


Figure 9: ASR in the block of MobileNet during the training phase.

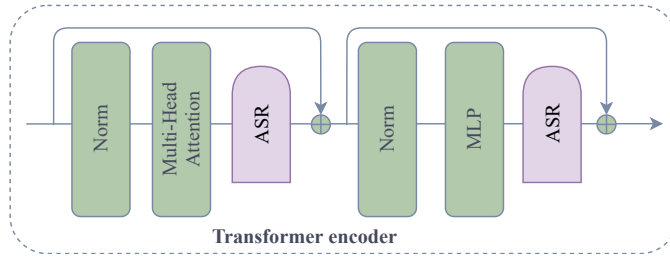


Figure 10: ASR in the transformer encoder of ViT during the training phase.

ResNet and ResNet-ACNet are popular convolutional neural network architectures that use basic blocks or bottlenecks. In our experiments, we insert ASR after the last batch normalization layer and before the residual addition operation, as shown in Fig. 6. We use Sigmoid as the activation function $\sigma(\cdot)$ of ASR, and we set the initial value of the learnable vector ψ to 0.1.

VGG and RepVGG are two VGG-type convolutional neural network architectures that are widely used in computer vision applications. In our experiments, we insert ASR between the batch normalization layer and ReLU activation function, as shown in Fig. 7. This location allows ASR to process the feature maps before they are passed to the next convolutional layer, which helps to reduce the batch noise (Liang et al. 2020) and distortion caused by the convolution. We use Sigmoid as the activation function $\sigma(\cdot)$ of ASR, and we set the initial value of the learnable vector ψ to 0.1.

ShuffleNetV2 is a lightweight convolutional neural network architecture that uses a dual-branch structure for its block. In our experiments, we insert ASR between the last batch normalization layer and ReLU activation function in the residual branch, as shown in Fig. 8. We use Sigmoid as the activation function $\sigma(\cdot)$ of ASR, and we set the initial value of the learnable vector ψ to 0.1.

MobileNet is another lightweight convolutional neural network architecture that uses depthwise and pointwise convolutional layers in each block. In our experiments, we insert ASR between BN and ReLU in both layers, as demonstrated in Fig. 9. This placement allows ASR to capture the non-linearity of both convolutional layers. We use Sigmoid as the activation function $\sigma(\cdot)$ of ASR, and we set the initial value of the learnable vector ψ to 0.1.

ViT. For ViT, we apply ASR to the transformer encoder, as illustrated in Fig. 10. ASR is inserted after multi-head attention and MLP. Moreover, distinct from other backbones, the transformer-based model ViT diverges from the conventional notion of channels. Instead, tokens and their associated features constitute the vectors from ViT. Therefore, we apply ASR to the dimension of the features. The activation function $\sigma(\cdot)$ employed within ASR is Tanh, and the initial value of the learnable vector ψ is set to $1e-3$. Correspondingly, the initial values of the network layers within ASR are also configured to $1e-3$.

D The initialization of ASR

In this section, we analyze the initialization of the input $\psi \in R^{C \times 1 \times 1}$ in ASR. We conduct experiments by initializing ψ with values ranging from 0.1 to 0.6 and evaluate the performance of ASR on the CIFAR100 dataset as shown in Table 13. Our findings suggest that an appropriate initialization value is crucial for the performance of ASR. Specifically, we find that ASR initialized with a value of 0.1 achieves the highest accuracy of 74.83% and 74.77% on the test set, while the accuracy of ASR with other initialization values varies from 74.03% to 74.73%. These results indicate that choosing an appropriate initialization value can significantly impact the performance of ASR, and initializing ASR with a value of 0.1 leads to the best performance on the CIFAR100 dataset.

Initialization	0.1	0.2	0.3	0.4	0.5	0.6
ASR (SE)	74.83	74.56	74.15	74.17	74.03	74.15
ASR (IE)	74.77	<u>74.55</u>	<u>74.73</u>	74.25	74.45	74.24

Table 13: Top-1 accuracy (%) of different initialization values on ASR’s performance. The backbone is ResNet83, and the dataset is CIFAR100. Bold and underline indicate the best results and the second best results, respectively.

E Different numbers of ASR inserted at the same position

In this section, we provide additional experimental results on the impact of inserting different numbers of ASR at the same position in ResNet164 and ViT. Specifically, we evaluate the performance of ResNet164 with 1, 2, 3, and 4 ASR modules inserted at the positions shown in Fig. 6. We report the top-1 and top-5 accuracy on the CIFAR100 validation set.

As shown in Table 14, for ResNet164, the performance generally improves as the number of ASR modules increases when $\delta < 3$. These results suggest that inserting multiple ASR modules at the same position in ResNet164 may further enhance the performance.

Module	$\delta = 1$		$\delta = 2$		$\delta = 3$		$\delta = 4$	
	Top-1 acc.	Top-5 acc.	Top-1 acc.	Top-5 acc.	Top-1 acc.	Top-5 acc.	Top-1 acc.	Top-5 acc.
ASR (SE)	75.36	93.53	75.87	93.99	75.72	94.15	75.22	93.56
ASR (IE)	75.58	93.84	75.71	93.81	75.45	94.07	74.56	93.73
ASR (SRM)	75.23	93.68	75.45	94.06	75.61	94.21	75.11	93.78
ASR (SPA)	75.12	93.44	75.43	93.66	75.81	94.03	75.62	93.46

Table 14: The accuracy (%) of ResNet164 with different numbers of ASR inserted at the same position on CIFAR100.

F The visualizations of the first-order difference (absolute value) for attention value over epoch

To provide further evidence for the claim made in our paper that most of the attention values almost converge at the first learning rate decay (30 epochs), we present additional visualizations of the first-order difference (absolute value) in attention value over epoch for different structures, attention modules, datasets, and training settings (including learning rate and weight decay). Each figure includes four subplots that show the evolution of attention value for different images. The horizontal axis indicates the number of epochs, while the vertical axis represents the order of random channel ID. Unless otherwise specified, we adopt ResNet83-SE as our baseline, CIFAR100 as the default dataset, and schedule learning rate as the default learning rate, with weight decay set to $1e-4$.

Different backbones. Fig. 11 and Fig. 12 show the first-order difference (absolute value) in attention value over epoch for ResNet83 and ResNet164, respectively. Both backbones exhibit the same trend, indicating that most of the attention values almost converge at the first learning rate decay (30 epochs).

Different attention modules. Fig. 11 and Fig. 13 present the first-order difference (absolute value) in attention value over epoch for two attention modules SE and IE, respectively. Although IE has some channel that converge more slowly than others, most of the channel attention values almost converge at 30 epochs.

Different datasets. Fig. 11 and Fig. 14 compare the attention values of ResNet83-SE on CIFAR100 and STL10 during the training process. Although ResNet83-SE exhibits greater attention value fluctuations in the initial stages on the STL10, our results still align with the findings presented in our paper.

Different training setting. We also compare the first-order difference (absolute value) in attention value over epoch for ResNet83-SE under different training settings. Fig. 11 and Fig. 15 show the results of using schedule learning rate and cosine learning rate, respectively. Fig. 16, Fig. 17, and Fig. 18 correspond to weight decay values of $2e-4$, $3e-4$, and $4e-4$, respectively. In all cases, we obtain results consistent with our paper’s findings. We also observe that larger weight decay values lead to faster attention value convergence.

G The results about the batch noise attack

We conduct experiments on three types of noise attacks to empirically verify the ability of ASR in regulating noise to improve model robustness, including batch noise, constant noise, and random noise. We consider the style transfer task, which generally adopts the instance normalization (IN) without batch noise, rather than BN, as adding batch noise would significantly reduce the quality of generated images due to noise interference.

In this section, we present additional results on the batch noise attack to support the conclusions of our paper. As shown in Fig. 19, Fig. 20, and Fig. 21, with batch noise (BN), there are more blurriness compared to without batch noise (IN). However, when ASR is applied to BN, the aforementioned issues are significantly reduced. This suggests that ASR can effectively alleviate the adverse effects of noise introduced by batch normalization, resulting in image quality comparable to that of IN without batch noise.

H The attention values of different images

In this section, we present additional examples to support the conclusions of our paper that after passing through the attention module, the channel attention values of different images tend to approach a certain value within the same channel, resulting in a “stripe structure”. We present in Fig. 22, Fig. 23, Fig. 24, Fig. 25, Fig. 26, Fig. 27, and Fig. 28 the visualization of attention values for different structures, attention modules, datasets, and training settings (including learning rate and weight decay values). The horizontal axis represents the order of random channels, while the vertical axis represents the order of random images. Corresponding to Appendix F, we use ResNet83-SE as the baseline, with the default dataset being CIFAR100, learning rate being schedule learning rate, and weight decay being $1e-4$. All figures show an obvious “stripe structure,” which is consistent with our conclusion in the paper that the attention values of different images tend to converge to a certain value within the same channel.

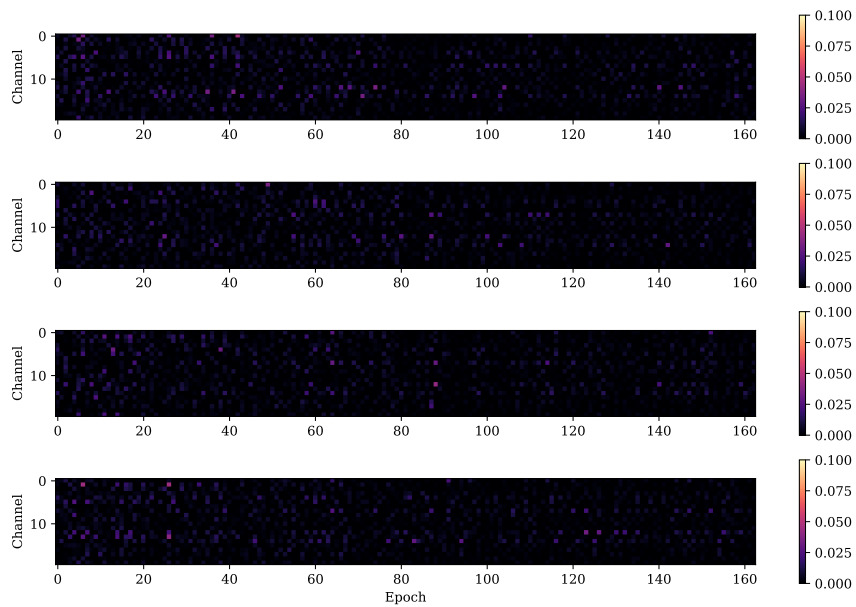


Figure 11: The visualization of the first-order difference (absolute value) for attention value of ResNet83-SE (weight decay: $1e-4$) over epoch on CIFAR100. Zoom in for best view.

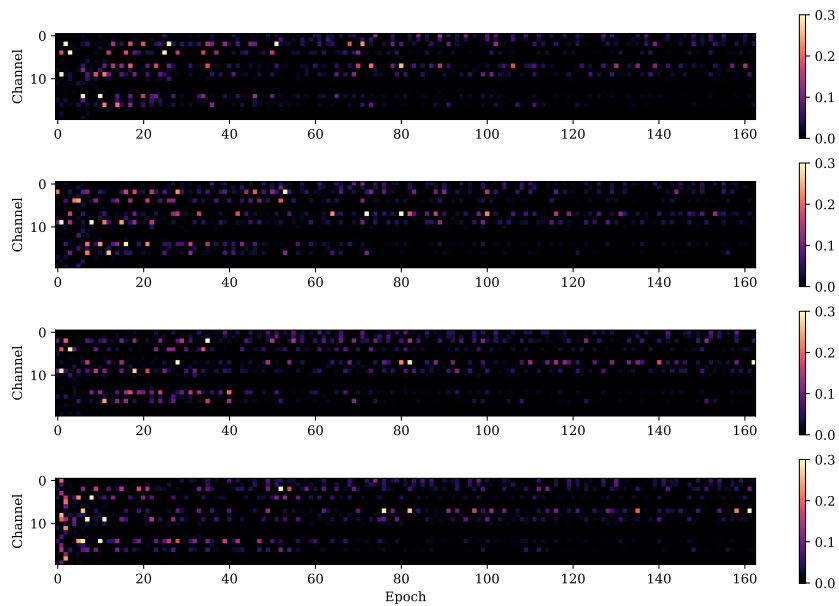


Figure 12: The visualization of the first-order difference (absolute value) for attention value of ResNet164-SE (weight decay: $1e-4$) over epoch on CIFAR100. Zoom in for best view.

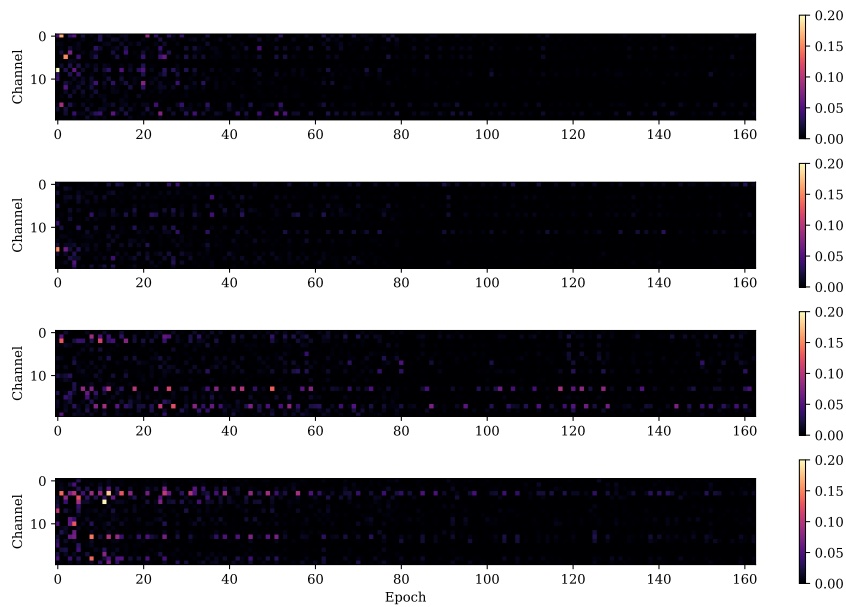


Figure 13: The visualization of the first-order difference (absolute value) for attention value of ResNet83-IE (weight decay: $1e-4$) over epoch on CIFAR100. Zoom in for best view.

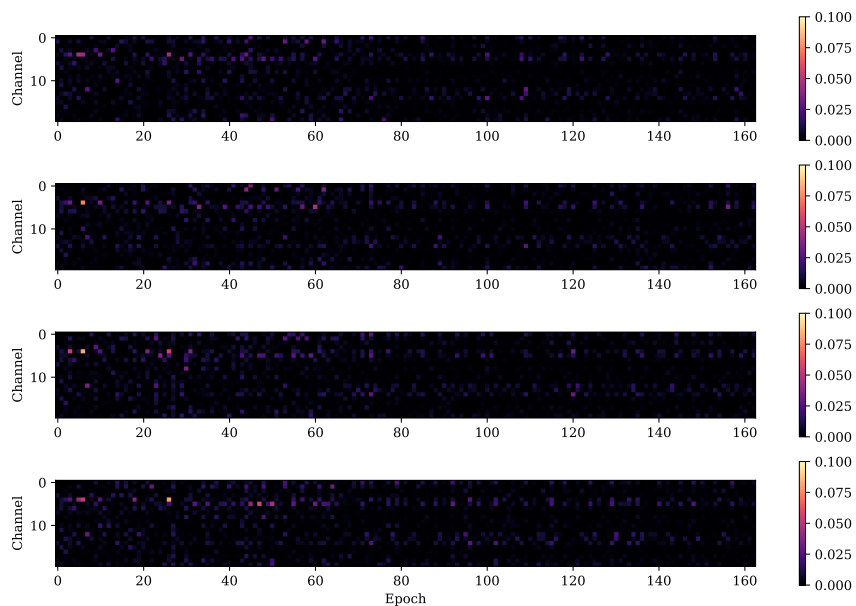


Figure 14: The visualization of the first-order difference (absolute value) for attention value of ResNet83-SE (weight decay: $1e-4$) over epoch on STL10. Zoom in for best view.

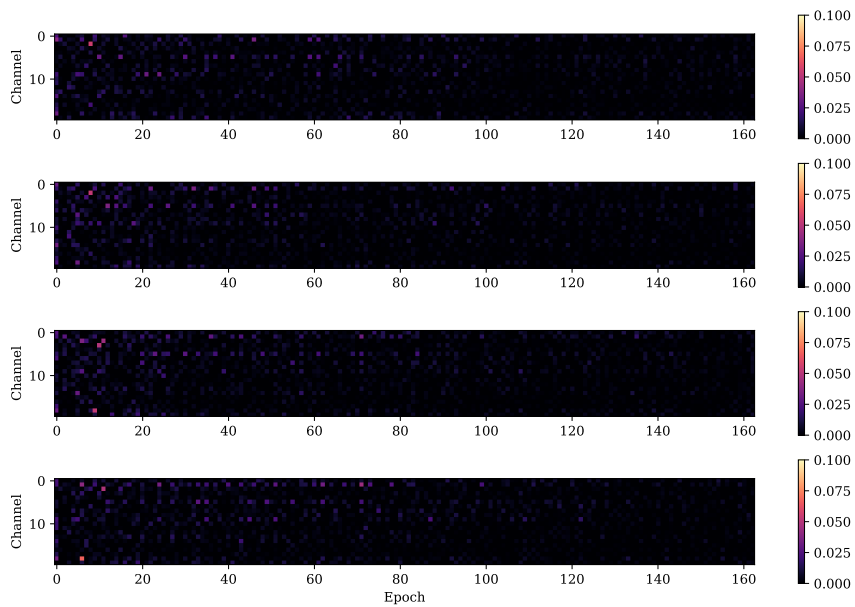


Figure 15: The visualization of the first-order difference (absolute value) for attention value of ResNet83-SE (weight decay: $1e-4$) based on cosine learning rate over epoch on CIFAR100. Zoom in for best view.

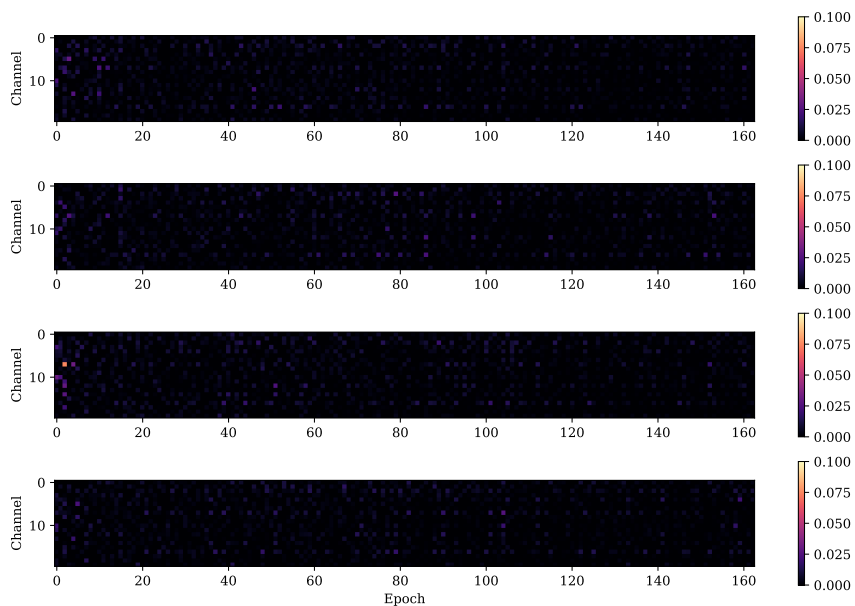


Figure 16: The visualization of the first-order difference (absolute value) for attention value of ResNet83-SE (weight decay: $2e-4$) over epoch on CIFAR100. Zoom in for best view.

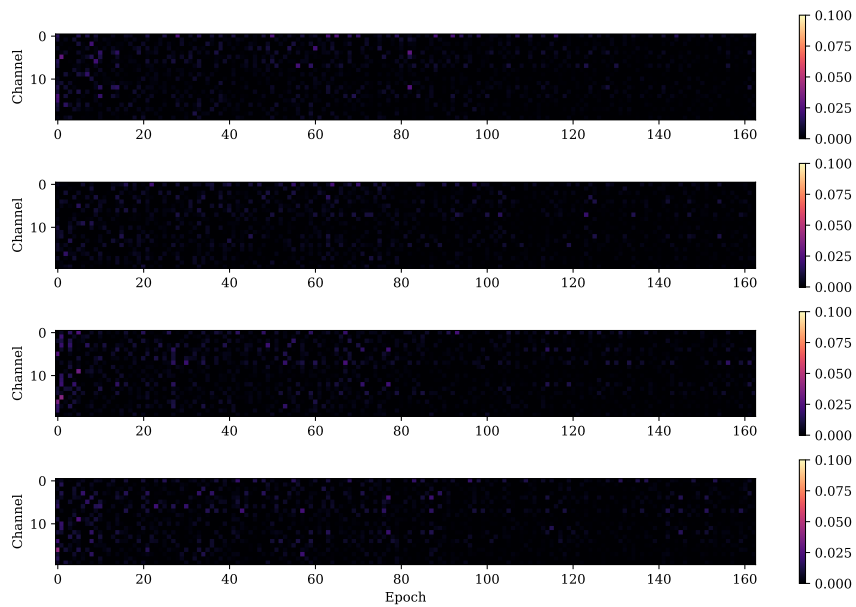


Figure 17: The visualization of the first-order difference (absolute value) for attention value of ResNet83-SE (weight decay: $3e-4$) over epoch on CIFAR100. Zoom in for best view.

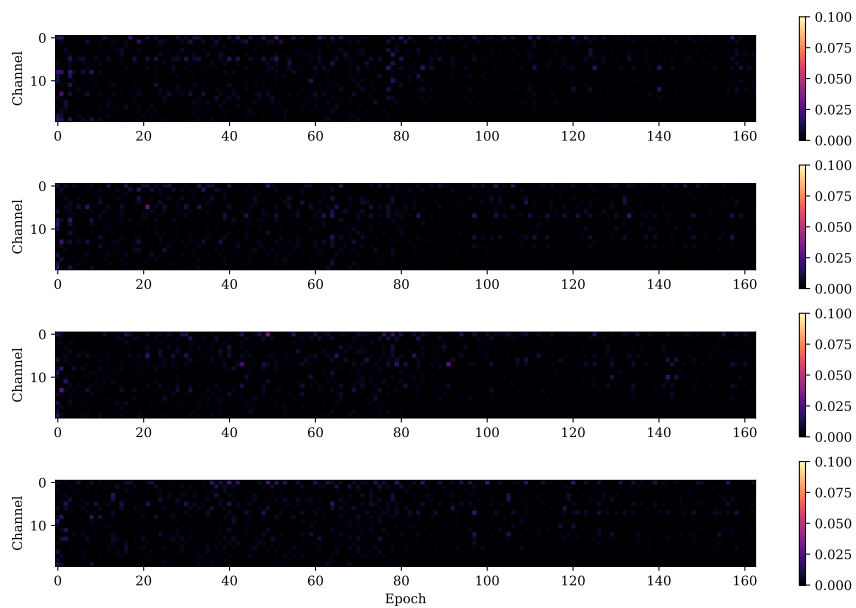


Figure 18: The visualization of the first-order difference (absolute value) for attention value of ResNet83-SE (weight decay: $4e-4$) over epoch on CIFAR100. Zoom in for best view.

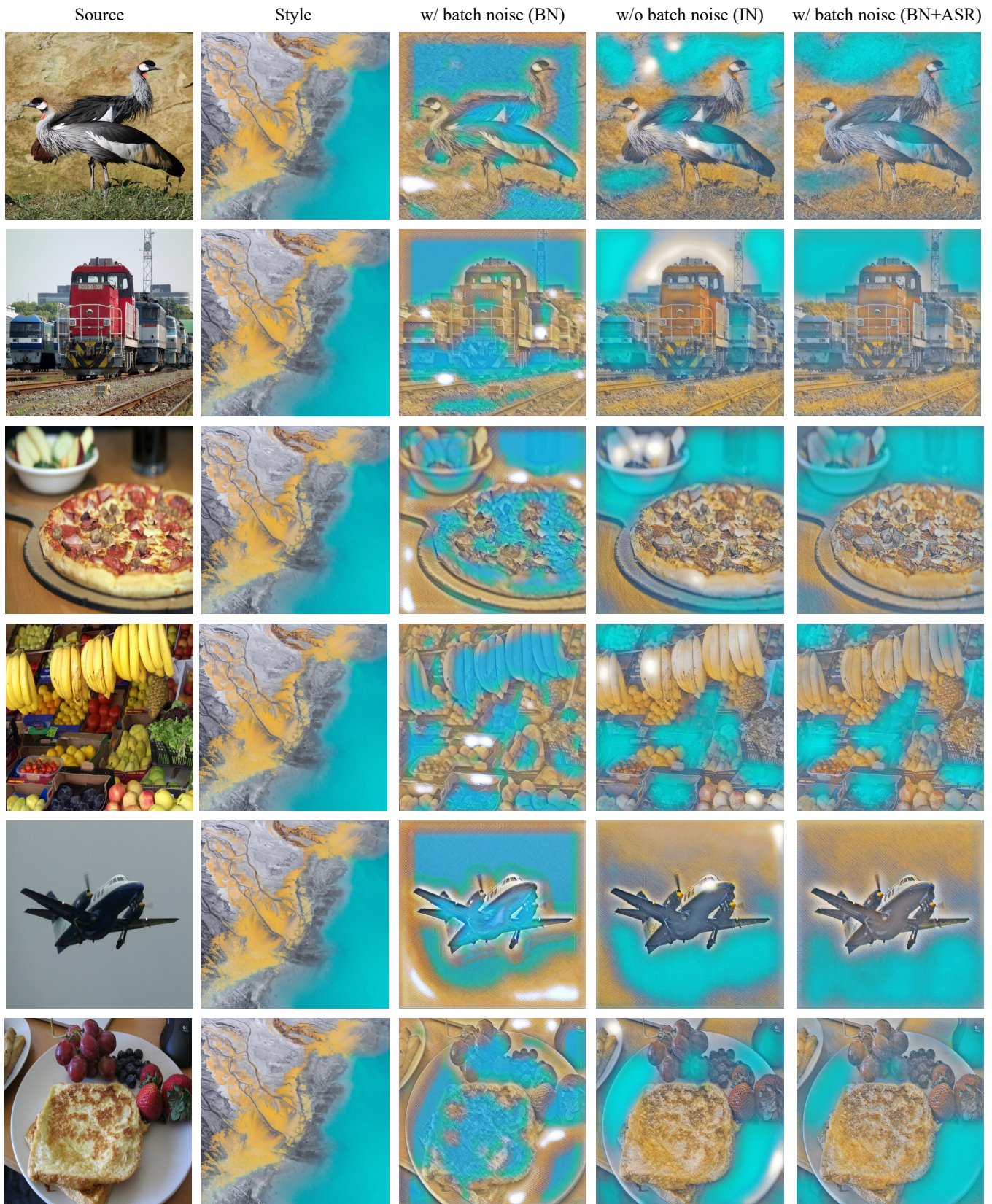


Figure 19: The results about the batch noise attack. Zoom in for best view.

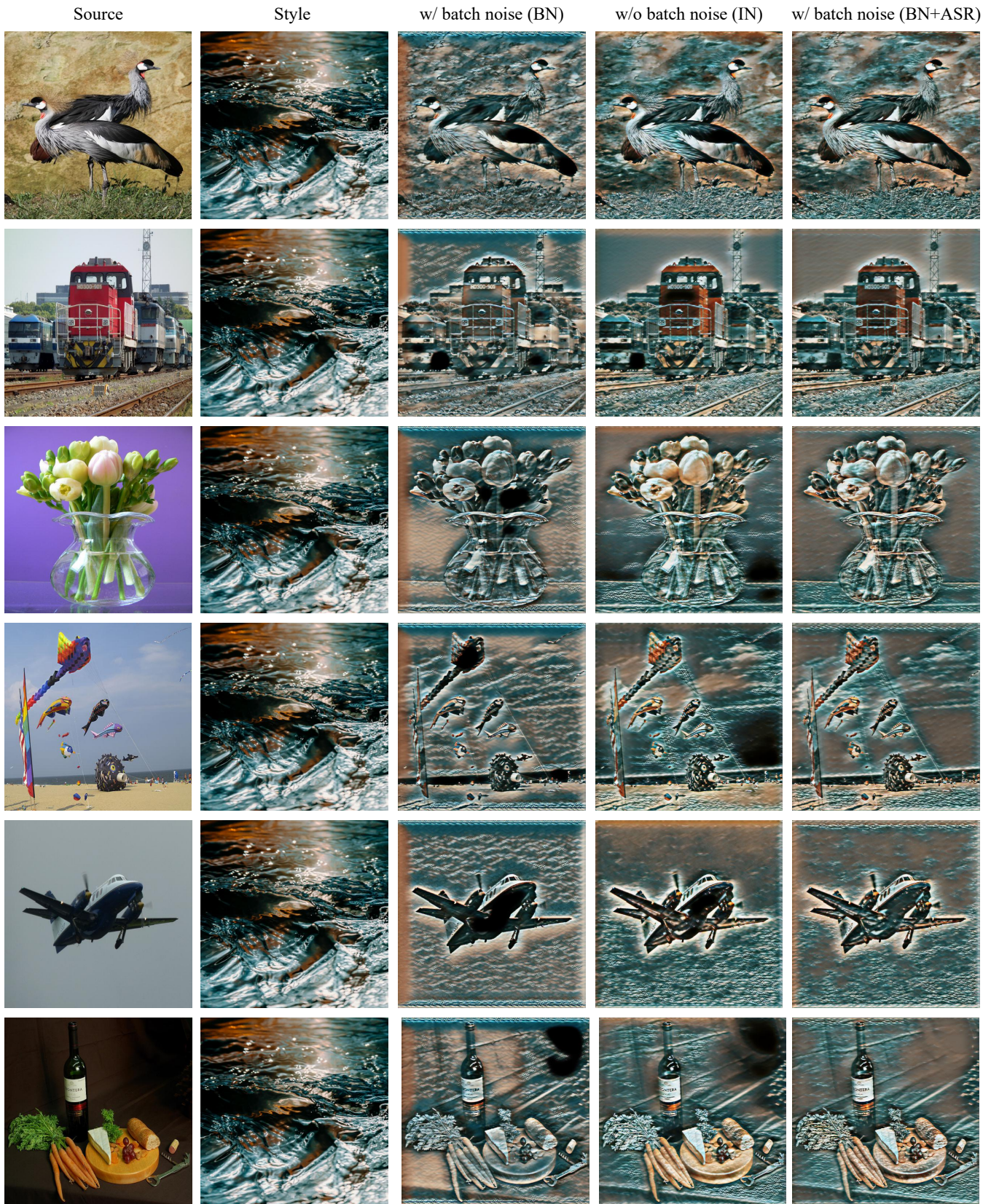


Figure 20: The results about the batch noise attack. Zoom in for best view.

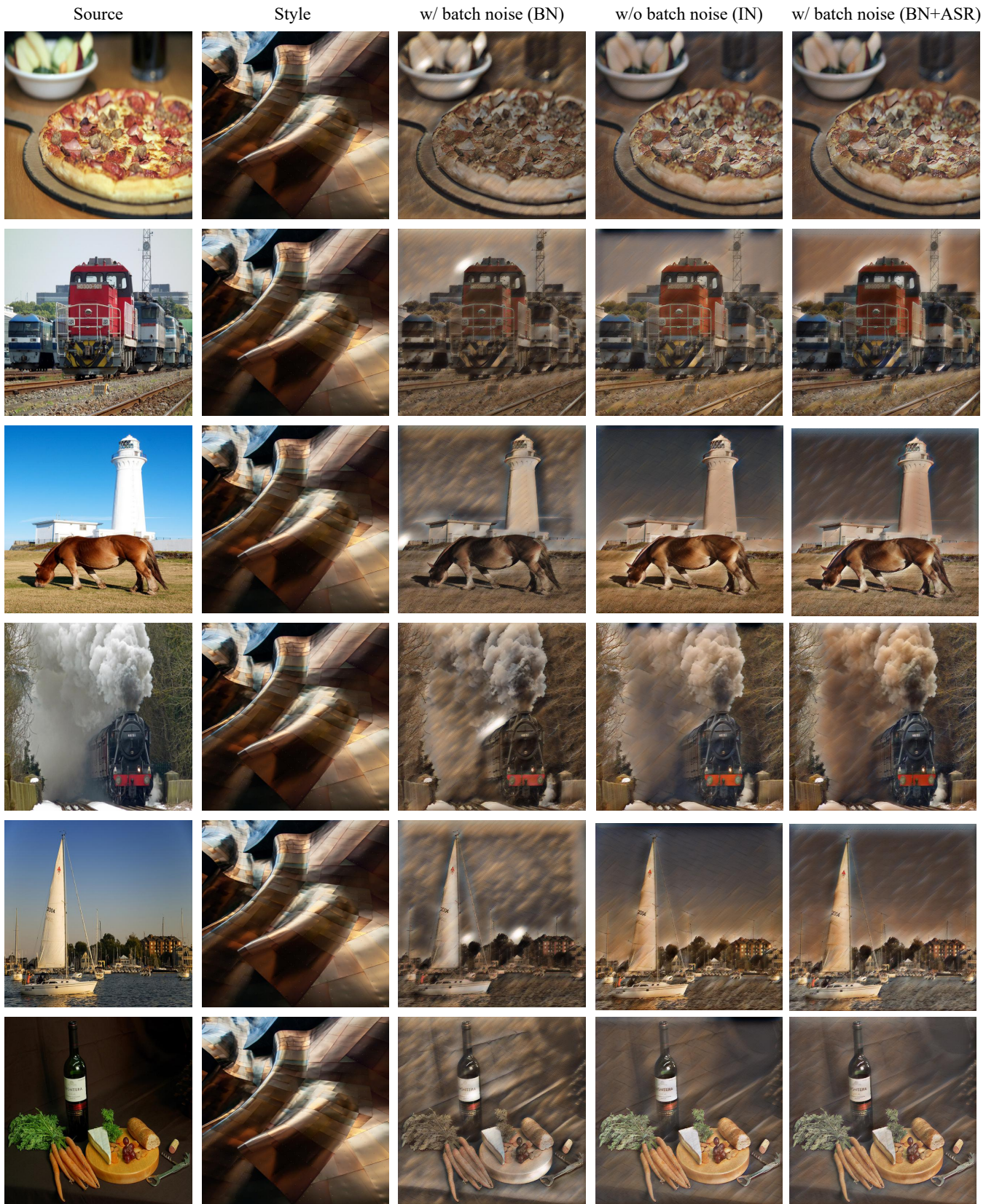


Figure 21: The results about the batch noise attack. Zoom in for best view.

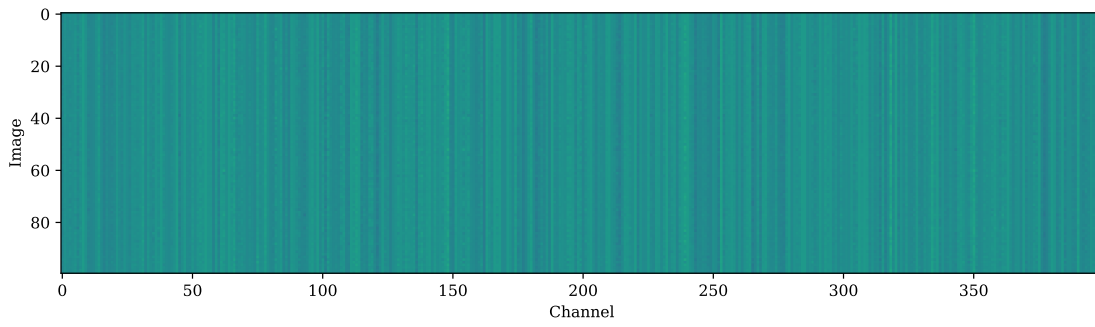


Figure 22: The attention values of different images from ResNet83-SE on CIFAR100. Zoom in for best view.

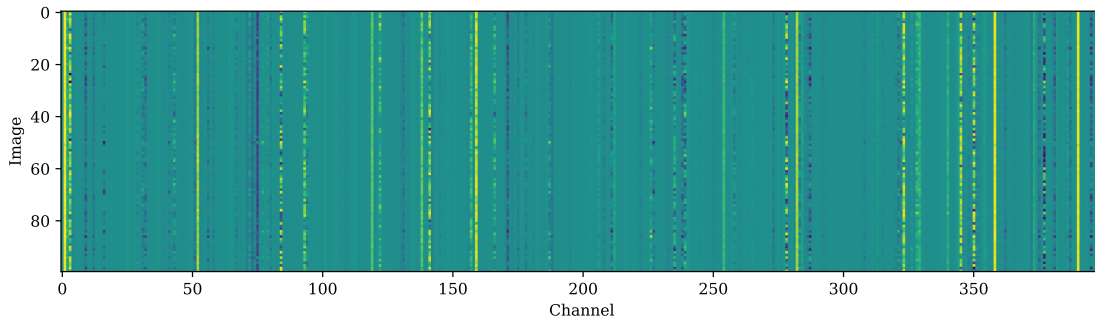


Figure 23: The attention values of different images from ResNet164-SE on CIFAR100. Zoom in for best view.

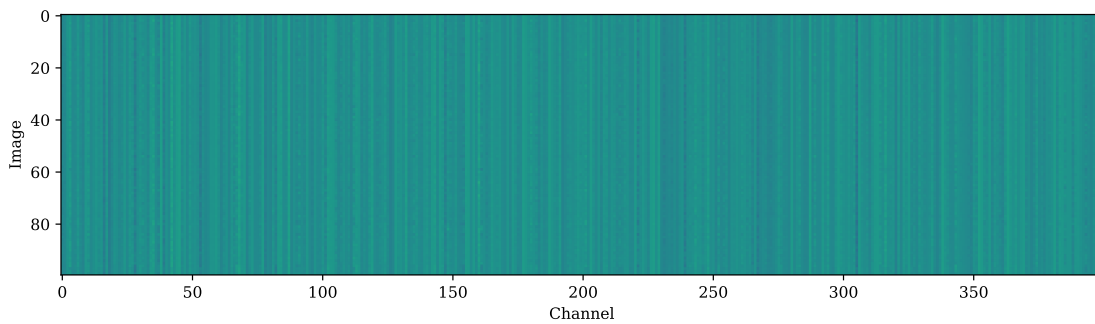


Figure 24: The attention values of different images from ResNet83-SE based on cosine learning rate on CIFAR100. Zoom in for best view.

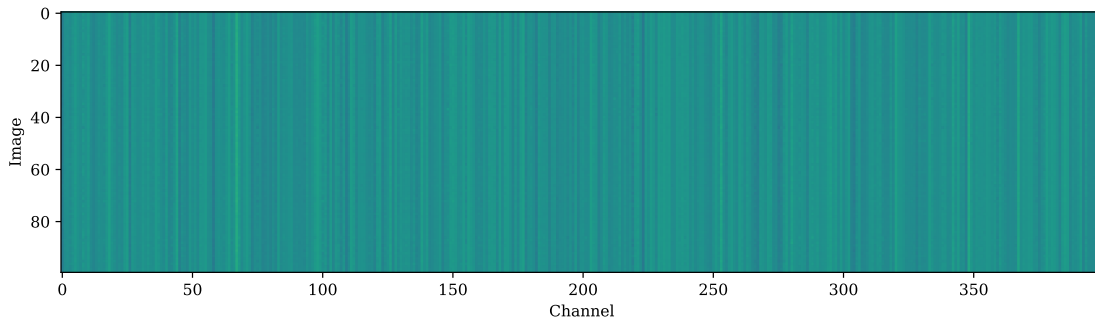


Figure 25: The attention values of different images from ResNet83-SE on STL10. Zoom in for best view.

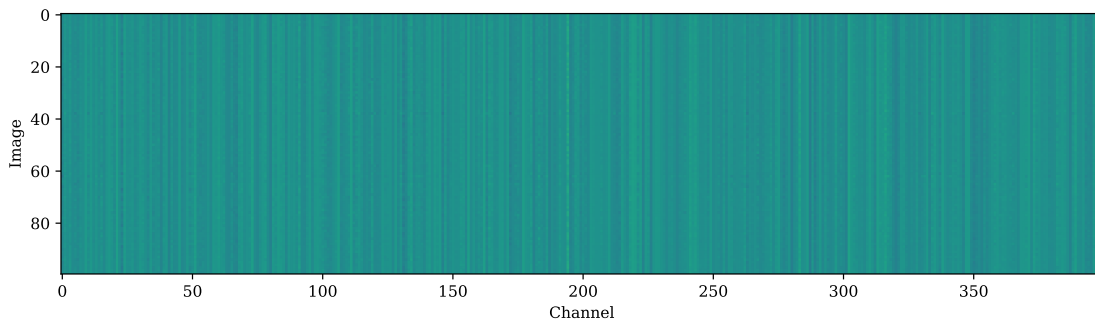


Figure 26: The attention values of different images from ResNet83-SE (weight decay: $2e-4$) on CIFAR100. Zoom in for best view.

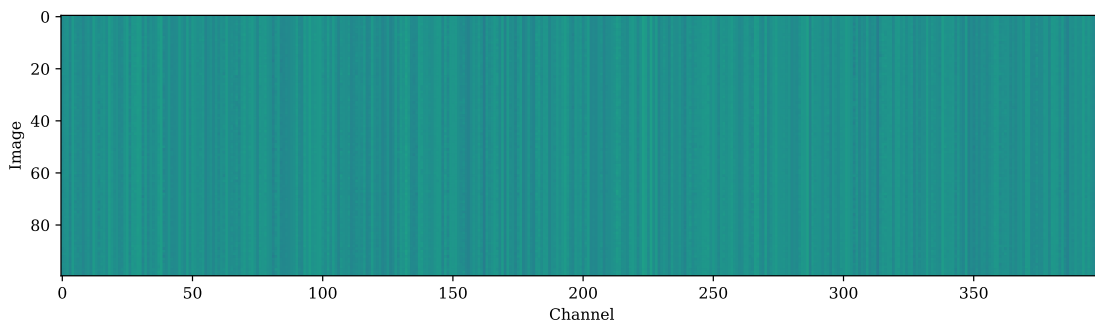


Figure 27: The attention values of different images from ResNet83-SE (weight decay: $3e-4$) on CIFAR100. Zoom in for best view.

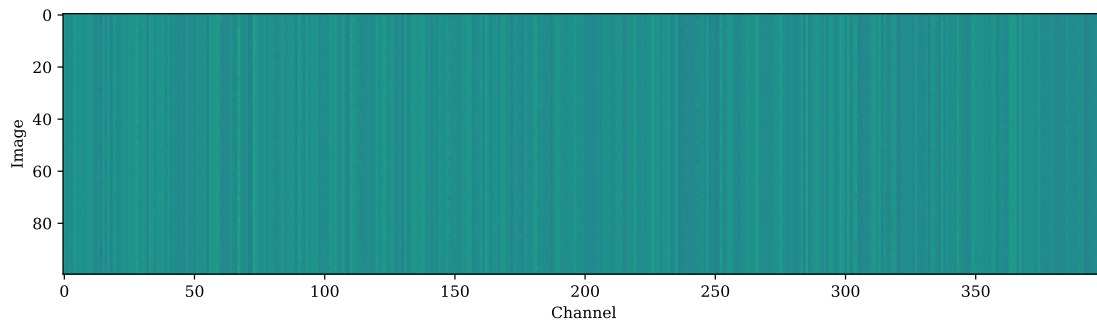


Figure 28: The attention values of different images from ResNet83-SE (weight decay: $4e-4$) on CIFAR100. Zoom in for best view.

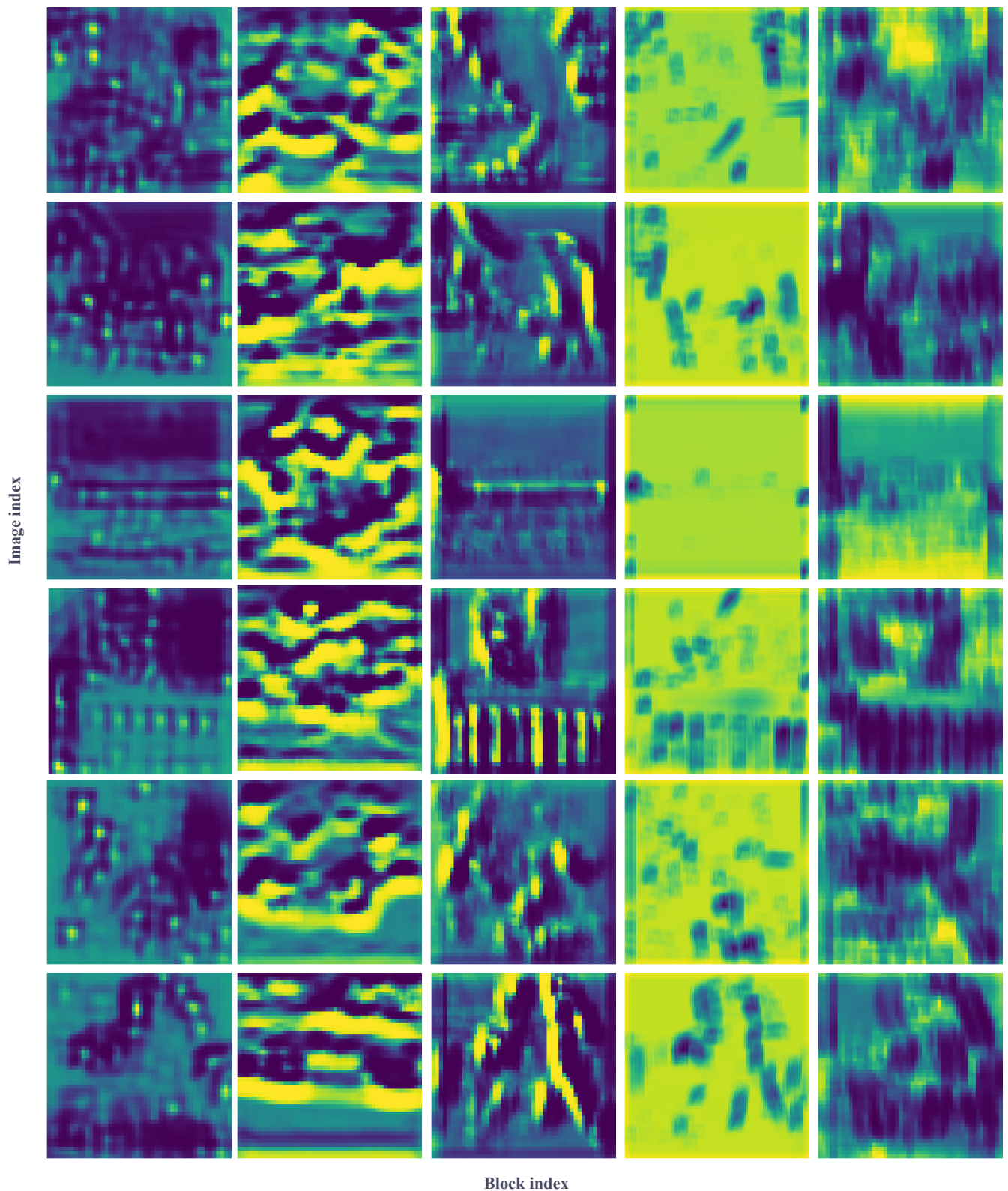


Figure 29: The visualization about the spatial attention from CBAM. We randomly select six images from STL10 and extract the spatial attention values of five blocks from ResNet83-CBAM. Each row in the visualization represents the spatial attention values of different blocks for the same image, while each column represents the spatial attention values of different images for the same block. Zoom in for best view.